Deep-Sea Research I 56 (2009) 1182–1202

Contents lists available at ScienceDirect

Deep-Sea Research I

journal homepage: www.elsevier.com/locate/dsri

The importance of tides for sediment dynamics in the deep sea—Evidence from the particulate-matter tracer ^{234}Th in deep-sea environments with different tidal forcing

Florian Peine [a,*], Robert Turnewitsch [b], Christian Mohn [c], Theresa Reichelt [d], Barbara Springer [a], Manfred Kaufmann [e]

[a] Department of Marine Biology, Biosciences, University of Rostock, Albert-Einstein-Str. 3, 18051 Rostock, Germany
[b] The Scottish Association for Marine Science, Dunstaffnage Marine Laboratory, Oban PA37 1QA, UK
[c] Department of Earth and Ocean Sciences, Martin Ryan Institute, National University of Ireland Galway, Ireland
[d] Institute of Oceanography, University of Hamburg, Bundesstr. 53, 20146 Hamburg, Germany
[e] Department of Biology & Centre of Macaronesian Studies, University of Madeira, Marine Biology Station of Funchal, Cais do Carvão 9000-107 Funchal, Madeira Island, Portugal

ARTICLE INFO

Article history:
Received 21 October 2008
Received in revised form
6 March 2009
Accepted 23 March 2009
Available online 9 April 2009

Keywords:
Thorium-234/uranium-238 disequilibria
Sediment dynamics
Bottom boundary layer
Topography
Seamounts
Internal tides
Northeast Atlantic
Eastern Mediterranean

ABSTRACT

Key aspects of deep-ocean fluid dynamics such as basin-scale (residual) and tidal flow are believed to have changed over glacial/interglacial cycles, with potential relevance for climatic change. To constrain the mechanistic links, magnitudes and temporal succession of events analyses of sedimentary paleo-records are of great importance. Efforts have been underway for some time to reconstruct residual-flow patterns from sedimentary records. Attempts to reconstruct tidal flow characteristics from deep-sea sediment deposits, however, are at a very early stage and first require a better understanding of the reflection of modern tides in sediment dynamics. In this context internal (baroclinic) tides, which are formed by the surface (barotropic) tide interacting with seafloor obstacles, are believed to play a particularly important role. Here we compare two modern deep-sea environments with respect to the effect of tides on sediment dynamics. Both environments are influenced by kilometre-scale topographic features but with vastly different tidal forcing: (1) two sites in the Northeast Atlantic (NEA) being surrounded by, or located downstream of, fields of short seamounts (maximum barotropic tidal current velocities $\sim$5 cm s^{-1}); and (2) a site next to the Anaximenes seamount in the Eastern Mediterranean (EMed) (maximum barotropic tidal current velocities $\sim$0.5 cm s^{-1}). With respect to other key fluid-dynamical parameters both environments are very similar. Signals of sedimentary particle dynamics, as influenced by processes taking place in the bottom boundary layer, were traced by the vertical water-column distribution of radioactive disequilibria (daughter/parent activity ratios $\neq 1$) between the naturally occurring, short-lived (half-life: 24.1 d) particulate-matter tracer ^{234}Th relative to its very long-lived and non-particle-reactive parent nuclide ^{238}U. Activity ratios of ^{234}Th/^{238}U < 1 in water samples collected near the seafloor indicate fast ^{234}Th scavenging onto particles followed by fast settling of these particles from the sampled parcel of water and, therefore, imply active sediment resuspension and dynamics on time scales of up to several weeks. In the Northeast Atlantic study region tides (in particular internal tides) are very likely to locally push total current velocities near the seafloor across the critical current velocity threshold for sediment erosion or resuspension whereas in the Eastern Mediterranean the tides are

* Corresponding author. Tel.: +49 381 4986056; fax: +49 381 4986052.
E-mail address: florian.peine@uni-rostock.de (F. Peine).

0967-0637/$ - see front matter
doi:10.1016/j.dsr.2009.03.009

much too weak for this to happen. This difference in tidal forcing is reflected in a difference of the frequency of the occurrence of radioactive disequilibria <1 between total ^{234}Th and ^{238}U: In the near-bottom water column of the Northeast Atlantic region 59% of samples had detectable ^{234}Th/^{238}U disequilibria whereas at the Eastern Mediterranean site this fraction was only 7% (including a few disequilibria >1). The results of this study, therefore, add to the evidence suggesting that tides in the deep sea of the open oceans are more important for sediment dynamics than previously thought. It is hypothesised that (a) tide/seamount interactions in the deep open ocean control the local distribution of erosivity proxies (e.g., distributions of sediment grain sizes, heavy minerals and particle-reactive radionuclides) in sedimentary deposits and (b) the aforementioned topographically controlled sedimentary imprints of (internal) tides are useful in the reconstruction of past changes of tidal forcing in the deep sea.

1. Introduction

Marine sedimentary deposits constitute one of the few natural archives of environmental change. Under certain circumstances fluid dynamics near the seafloor may become sufficiently intense to influence sediment transport and deposition (e.g., Ziervogel and Bohling, 2003; McCave and Hall, 2006). Understanding the impact of fluid dynamics on sediment deposition is, therefore, an essential prerequisite for (1) the interpretation of sedimentary records (e.g., Francois et al., 2004, 2007; Kienast et al., 2007; Lyle et al., 2005, 2007; Broecker, 2008) and (2) the use of sediment-based proxies for the reconstruction of past changes of aspects of fluid dynamics in the deep sea (e.g., McCave and Hall, 2006).

Different fluid-dynamical components combine to form the overall flow in the deep sea. So-called benthic storms (comparatively high near-seafloor current velocities of O(10 cm s^{-1}) (the symbol O(…) stands for 'on the order of') lasting for at least a few days and possibly being associated with passing meso-scale eddies; e.g., Gross and Williams, 1991) and turbidity currents (rapidly moving, sediment-laden water moving down a slope; e.g., Seibold and Berger, 1993) are highly energetic events with the potential to transport significant amounts of particulate material in a relatively short time.

Temporally more continuous fluid-dynamical components are residual flow (mean current without periodic components), tides and internal waves. At a given location and time they are less energetic than benthic storms or turbidity currents. However, there is evidence that under certain circumstances they may become sufficiently strong, over longer time scales, to affect sediment dynamics. In the following we focus on these less energetic but more continuous fluid-dynamical components.

How exactly basin-scale (residual) flow has changed in the deep ocean over time scales of 100 s up to 100,000 s of years is a subject of ongoing work (e.g., see overviews by Lynch-Stieglitz et al., 2007; van Aken, 2007). In addition, Egbert et al. (2004) provided model-derived evidence for glacial/interglacial sea-level-related changes of tidal kinetic energy and dissipation of tidal energy (one of the main energy sources for the formation of the internal-wave field and vertical mixing in the interior ocean; Wunsch and Ferrari, 2004) in the deep ocean. Kienast et al. (2007) propose changing deep sea tidal current flow during the past 30,000 years as one possible explanation for the sedimentary patterns they find in the Panama Basin. The mechanistic link between ocean overturning and mixing could possibly be of importance but has remained unclear so far (e.g., Nilsson et al., 2003; Wunsch and Ferrari, 2004; Montenegro et al., 2007).

A sediment-based approach for the reconstruction of past changes of residual flow and tidal forcing in the deep ocean would, therefore, be of great help in resolving the interconnections and temporal succession of fluid-dynamical changes within the context of climate change. As one of the first steps towards this goal a thorough understanding of the impact of modern fluid dynamics on the most recent sedimentary deposits is required. In this context a major challenge is to separate the signals of changing residual and tidal flow in the sedimentary record.

McCave and Hall (2006) reviewed the sedimentological sortable-silt-size approach for reconstruction of paleo-flow speeds that has been interpreted to mainly reflect past changes of residual flow. A new and independent approach which may help reconstruct past changes of residual flow could be based on the work of Turnewitsch et al. (2004). It utilizes the reflection of asymmetric flow fields associated with kilometre-scale topographic elevations of comparable breadth and width (seamounts) in the underlying sedimentary record. Because of conservation of potential vorticity even a perfectly symmetric seamount in, for example, the northern hemisphere would be surrounded by asymmetric flow fields with increased current velocities on the left side of the topography looking downstream (e.g. Gould et al., 1981; Chapman and Haidvogel, 1992; Goldner and Chapman, 1997; Beckmann and Mohn, 2002; Mohn and Beckmann, 2002). If, at least in some sectors of the topographically controlled flow field, the near-seafloor current velocities are sufficiently high [$\sim>$(6.5–10.5)cm s^{-1}] (Lampitt, 1985; Ziervogel and Bohling, 2003) to erode or resuspend sediment the flow-field asymmetry is reflected in the underlying sediments (Turnewitsch et al., 2004). The extent and orientation of the asymmetry are expected to be measures for the current velocity and direction of the residual flow, respectively. Consequently, down-core changes in the horizontal pattern of erosivity proxies in the sedimentary

record around the seamount should reflect paleo-changes in the velocity and orientation of the ambient residual flow.

Superimposed on the residual-flow pattern is the flow pattern caused by the interaction of the barotropic tide with the topography (e.g., Goldner and Chapman, 1997). The geometry of the flow field that results from the tide/topography interaction depends on the position of the system within the parameter space of topographic slope criticality and Froude number (or 'excursion parameter').

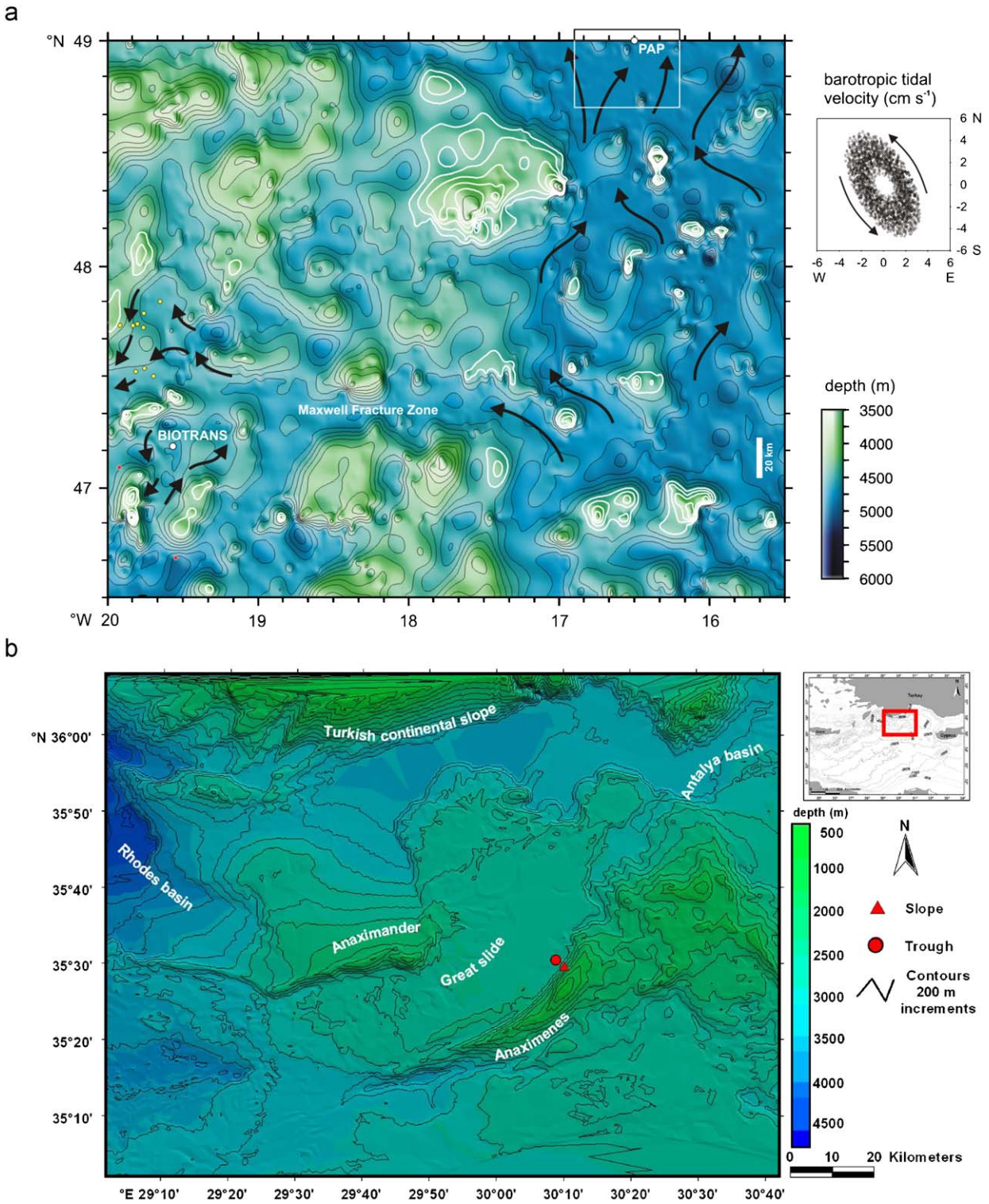

If (near-)critical topographic slopes occur together with Froude numbers $\ll 1$ the interaction of the barotropic tide leads to formation of internal (baroclinic) tides (e.g., St. Laurent and Garrett, 2002; Vlasenko et al., 2005; Garrett and Kunze, 2007).

The criticality, C, of a topographic slope is given by the ratio of the slope of the topography, ∇h, and the wave characteristic $s = ((\omega_0^2 - f^2)/(N^2 - \omega_0^2))^{0.5}$, where f is the Coriolis parameter, ω_0 is the frequency of the barotropic tide, and N is the buoyancy frequency: $C = |\nabla h|/s$. For $C<1$, $C=1$, and $C>1$ the topography is subcritical, critical, and supercritical, respectively. The criticality parameter is relevant within the context of topographically controlled sediment dynamics because (near-)critical slope sections are associated with the formation of internal tides and, therefore, particularly intense fluid dynamics and locally increased current velocities near the seafloor.

Here the Froude number (or 'excursion parameter') represents the ratio of the measure of the tidal excursion, U_0/ω_0, to the horizontal topographic length scale, k^{-1} (e.g., Garrett and Kunze, 2007). U_0 is the amplitude of the barotropic tidal current velocity and ω_0 is the frequency of the barotropic tide. The horizontal scale of the topography, k^{-1}, is the reciprocal value of the horizontal wave number, k, of the bathymetry (a measure for the number of topographic features per unit of distance).

The now accepted explanation for the formation of internal tides is that they are generated by the interaction of the barotropic surface tide with bottom topography. As the depth-independent barotropic (surface) tide sweeps stratified water over topographic features, it disrupts isopycnal layers, generating pressure gradients that induce secondary internal motions at the same frequency as the tide (e.g., Ray, 2001; Garrett and Kunze, 2007).

On (near-)critical slope sections where the internal-tide beams emanate, near-seafloor current velocities are predicted to be particularly high, increasing the likelihood of sediment erosion or resuspension. Evidence for the importance of internal tides for sediment dynamics has been found for locations near the continental rise, on continental slopes and at shelf breaks (Dickson and McCave, 1986; Cacchione et al., 2002). Moreover, recent work by Turnewitsch et al. (2008) provides evidence for the importance of internal tides for sediment dynamics in the abyssal ocean away from continental margins in regions structured by abyssal hills and short seamounts (Fig. 1a). This latter work suggests that, in larger parts of the deep sea, tides, and in particular internal tides, may be essential for controlling the formation of the sedimentary record. This is because it is the tides that locally push the overall current velocities over the estimated critical current velocity threshold of $\sim(6.5–10.5)\,\mathrm{cm\,s^{-1}}$ for surface-sediment erosion or resuspension (Turnewitsch et al., 2008). It is, therefore, very likely that, at least in certain regions of the deep ocean, tides leave a sedimentary imprint in sediments surrounding short seamounts and perhaps also in locations where internal-tide beams reflect from the seafloor (it is worth noting that the latter may be well away from topography).

Sedimentary deposits controlled by kilometre-scale flow-topography interactions seem to have a high potential of recording past changes of both residual flow and tidal forcing. The challenge now is to separate the signals of residual and tidal flow in the topographically controlled sedimentary records. This requires more work on the relation between modern residual flow and tides on the one hand and their reflection in the most recent sedimentary dynamics and deposits on the other hand.

In this context the present study, building on the work of Turnewitsch et al. (2008), searches for further evidence for the importance of tides for sediment dynamics in the deep sea. This is accomplished by comparing the water-column distribution of a naturally occurring particulate-matter tracer (thorium-234 or ^{234}Th) near kilometre-scale topography between two deep-sea environments in the Northeast Atlantic (NEA) and the Eastern Mediterranean (EMed). In terms of all key fluid-dynamical parameters these two environments are very similar. The main exception is the tidal forcing. The barotropic tidal current velocities differ by about one order of magnitude, with the EMed having the weaker tidal forcing. If a difference in ^{234}Th-inferred particle dynamics between these two environments is found, it must be attributed to the effect of tidal forcing. As we will show the results provide further evidence for tides being more important for sediment dynamics in the deep sea than previously thought.

2. Study regions, material and methods

2.1. Study regions

This work is based on the comparison between study regions in the NEA and EMed. The NEA samples were collected on the Porcupine Abyssal Plain (PAP) (seafloor at ~4800 m depth; 49.0°N, 16.5°W) and at the BIOTRANS site (seafloor at ~4550 m depth; 47.18°N, 19.57°W) on the eastern flank of the Mid-Atlantic Ridge (Fig. 1a). The PAP site is downstream of a field of short seamounts whereas the BIOTRANS site is surrounded by short seamounts. The average height of these seamounts relative to the seafloor at the sampling sites is ~600 m (range: ~200 up to

Fig. 1. (a) Bathymetric map (based on Smith and Sandwell, 1997) of the Northeast Atlantic study region with BIOTRANS and Porcupine Abyssal Plain (PAP) sites indicated (modified after Turnewitsch et al., 2008). White isobaths: heights of 400–800 m above the seafloor (the approximate core of the layer of 'fossil' disequilibria) relative to the Porcupine Abyssal Plain (nominally at 4800 m depth) and the BIOTRANS site (nominally at 4650 m depth). Yellow dots: current-meter positions of the NOAMP program. Red dots: deep-water stations sampled for ^{234}Th by Ken Buesseler et al. (unpublished; WHOI) during the NABE. Black arrows: near-seafloor flow field as interpreted from published (Dickson et al., 1985; Mittelstaedt et al., 1986; Klein and Mittelstaedt, 1992; McCartney, 1992; Castro et al., 1998) and unpublished information. The ellipse of barotropic tidal current vectors at the PAP site is also shown (based on the model of Egbert and Erofeeva (2002); data points are plotted based on an hourly resolved time series covering 1 April 2000, 00:00–30 June 2000, 00:00). (b) Bathymetric map of the Anaximander Mountains in the Eastern Mediterranean (based on the data set of ten Veen et al., 2004). Sampled stations are indicated by a circle (trough station) and a triangle (slope station). The small map shows the location of the study region in the Eastern Mediterranean.

~1100 m) (Mittelstaedt et al., 1986; Klein and Mittelstaedt, 1992; Smith and Sandwell, 1997). In the EMed work focused on the Anaximenes seamount, which is one of the three peaks of the Anaximander Mountains located in the northern Levantine Basin ~100 km south of Turkey and ~200 km west-northwest of Cyprus (Fig. 1b). The group of mountains is bordered by the deep Rhodes basin (seafloor at ~4500 m depth) in the west and the shallower Antalya basin (seafloor at ~2600 m depth) in the east. The Anaximenes seamount is the central elevation of the Anaximander Mountains with water depths at the base between ~2000 and 3000 m; the minimum summit depth is ~700 m (ten Veen et al., 2004).

2.2. Sampling

Relevant aspects of the physical oceanography of the study region in the NEA were reviewed by Turnewitsch et al. (2008) and, for comparative purposes, are summarised in Section 3.1. In December 2006 a combined hydrographic and biogeochemical survey was carried out at Anaximenes Seamount in the EMed onboard R.V. *Meteor* (cruise M71/1).

Hydrographic and biogeochemical properties of the water column were sampled at two different stations using a 23-bottle Seabird-Systems® CTD-rosette. Station "slope" was located on the lower slope and station "trough" over a slope-parallel channel at the base of the seamount (Fig. 1b). The slope site was sampled six times: twice shortly after neap tide, twice between neap and spring tide, and twice at spring tide. The trough site was sampled four times: twice between neap and spring tide, and twice shortly before spring tide (Fig. 2 and Table 1). Each sampling couple consists of a situation of roughly upslope and a situation of roughly downslope tidal flow.

In addition, two ship-mounted acoustic Doppler current profiler (ADCP) systems were operated during the cruise to measure the three-dimensional flow field at and around the seamount. The primary instrument was an RDI 75 kHz Ocean Surveyor system (bin length 16 m, maximum range 600 m), which was in operation for the first 7 d of the cruise. It was replaced by a RDI 38 kHz Ocean Surveyor system (bin length 16 m, maximum range 800 m) thereafter. Because of technical problems both systems could not be operated simultaneously. ADCP data post-processing was carried out using the Common Oceanographic Database Access System (CODAS3) shipboard ADCP processing suite (Firing et al., 1995). The main processing steps included 5-min ensemble averaging of the raw data, rotation from transducer to earth coordinates and a quality analysis to identify data gaps and navigational errors. Absolute current velocities were calculated by removing the ship velocity relative to an oceanic reference layer (ADCP bins 5–12) from the ship velocity over the ground at each depth bin. Finally, the Oregon State University (OSU) tidal model output (Egbert and Erofeeva, 2002) was used to separate barotropic tidal and residual currents in each velocity profile.

Weekly composites of dynamic topography (cm) and geostrophic currents (cm s^{-1}) from AVISO satellite altimetry (www.aviso.oceanobs.com) were used to analyse

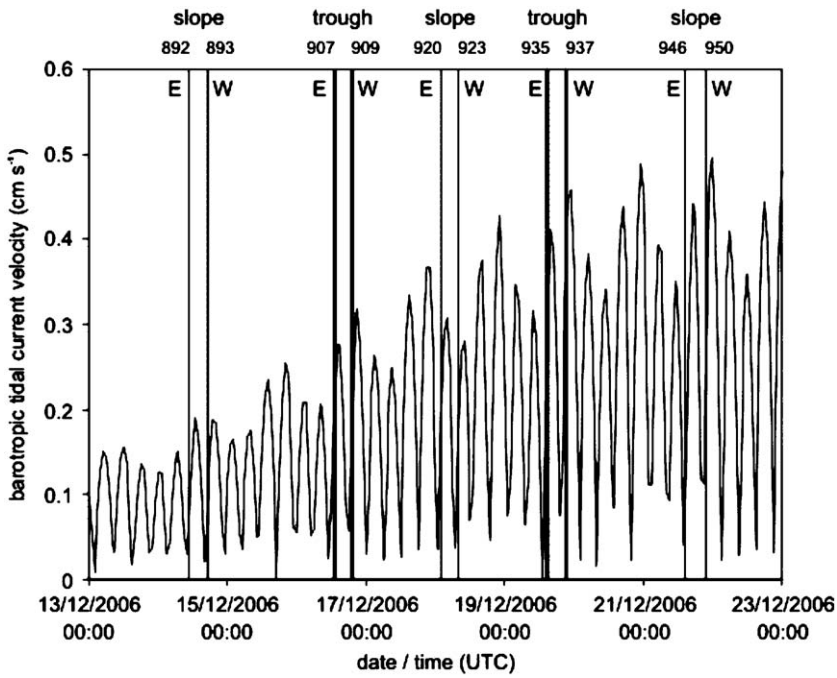

Fig. 2. Hourly resolved time series of the barotropic tidal current velocity near the ^{234}Th sampling sites in the Eastern Mediterranean (based on the OSU inverse tidal model of Egbert and Erofeeva, 2002). The time series covers the time interval during which ^{234}Th samples were collected. The sampling times and corresponding CTD deployment numbers are indicated. E (eastward) and W (westward) indicate the prevailing directions of the barotropic tidal current during sample collection.

Table 1
Sampling times, IDs of CTD deployments, station names, sampling locations and total water depths for CTD bottle sampling.

Sampling date/time (UTC)	CTD #	Station	Latitude (N)	Longitude (E)	Total water depth (m)
12 Dec 2006/16:30	881	Rhodes basin	35°55.0′	28°48.0′	4429
14 Dec 2006/10:43–11:09	892	Slope	35°29.5′	30°10.1′	1771
14 Dec 2006/17:02–17:29	893	Slope	35°29.5′	30°10.1′	1771
16 Dec 2006/12:43–13:23	907	Trough	35°30.2′	30°9.0′	2125
16 Dec 2006/18:53–19:24	909	Trough	35°30.2′	30°9.0′	2125
18 Dec 2006/01:39–02:08	920	Slope	35°29.5′	30°10.1′	1551
18 Dec 2006/07:46–08:17	923	Slope	35°29.5′	30°10.1′	1766
19 Dec 2006/14:36–15:10	935	Trough	35°30.2′	30°9.0′	2125
19 Dec 2006/21:09–21:38	937	Trough	35°30.3′	30°9.0′	2125
21 Dec 2006/14:14–14:43	946	Slope	35°29.5′	30°10.1′	1771
21 Dec 2006/21:39–22:14	950	Slope	35°29.5′	30°10.1′	1771

Sampling depths and heights above the seafloor can be found in Table A1.

the dominant features and variability patterns of surface currents in the EMed for a period of 8 weeks (mid-November 2006–mid-January 2007) centered around the field-work survey period. These AVISO parameters represent multimission altimeter products on a 1/8° regular grid.

For the comparison of the physical oceanographic information from the NEA and the EMed it needs to be kept in mind that different techniques were used and different time scales were sampled. The majority of flow-field information from the NEA comes from current-meter measurements from the deep water column whereas for the EMed it comes from ADCP measurements near the seamount summit. Also, the sampling intervals for the NEA are on a time scale of months whereas for the EMed the time scale is only days.

2.3. The particle tracer ^{234}Th

2.3.1. Background

We use the vertical water-column distribution of a naturally occurring particulate-matter tracer with a well-defined source and known half-life similar to the characteristic time scale of tides as a proxy for sediment dynamics near seafloor topography. This, in turn, indirectly bears information on topography-related fluid dynamics. The tracer, thorium-234 (^{234}Th), is a highly particle-reactive radionuclide with a short half-life of $t_{1/2} = 24.1$ d (decay constant: $\lambda_{Th} = \ln 2/t_{1/2} = 0.02876\,\mathrm{d}^{-1}$). It can, therefore, be concluded that ^{234}Th distributions reflect quasi-integrative processes of particle dynamics that occurred on a time scale of up to several weeks before sampling. One mean life of ^{234}Th ($1/t_{1/2} = 34.8$ d) comprises ~70 semi-diurnal tidal cycles and more than two complete tidal neap–spring cycles. Consequently, ^{234}Th is a particularly suitable tracer for studying tidally controlled sediment dynamics. Thorium-234 has been successfully used as a particulate-matter tracer in the near-bottom water column of open-ocean environments in a few studies (Bacon and Rutgers van der Loeff, 1989; DeMaster et al., 1991; Turnewitsch and Springer, 2001; Rutgers van der Loeff et al., 2002; Inthorn et al., 2006).

Several processes control the ^{234}Th distribution. Thorium-234 is produced by radioactive decay of its very long-lived (half-life: 4.468×10^9 yr) and chemically conservative (not particle-reactive) parent ^{238}U and has a reasonably well-constrained sorptive behavior (e.g., Bacon and Anderson, 1982; Honeyman et al., 1988; Quigley et al., 2001; Geibert and Usbeck, 2004). The distribution of ^{234}Th does not seem to be significantly controlled by processes other than ^{238}U decay, its own radioactive decay, net adsorption onto particulate matter, and particulate-matter settling.

Distributions of ^{234}Th can convey information on fluid dynamics at the seafloor. Sediment erosion may result in particulate-matter resuspension, which, in turn, may lead to scavenging of dissolved ^{234}Th from the near-bottom water column. If, for a given parcel of water, the scavenging rate of ^{234}Th onto particles and the rate of ^{234}Th export on settling particles from the water parcel are high in comparison to ^{234}Th production by ^{238}U decay, a radioactive disequilibrium occurs. This means the radioactivity of total (particulate+dissolved) ^{234}Th is less than the ^{238}U radioactivity. Hence, the spatial distribution of total ^{234}Th relative to the parent nuclide ^{238}U may convey information on the intensity of sediment dynamics, erosiveness and, indirectly, the fluid dynamics in the vicinity of a sampling site.

2.3.2. Laboratory procedures

Thorium-234 was sampled at strategically chosen times during one half of a neap–spring tidal cycle (Fig. 2). To be able to allocate these sampling times to specific parts of the neap–spring, diurnal and semi-diurnal tidal cycle the barotropic tides were predicted for the time just before, during and just after the cruise using the Mediterranean Sea regional solution (1/12° resolution) of the OSU inverse tidal model described in Egbert and Erofeeva (2002). Slope and trough stations were sampled as outlined in Section 2.2. Vertical sampling resolution for the bottle samples was increased within the bottommost ~50 m and decreased further up in the water column.

Analytical procedures for total ^{234}Th in the NEA were described by Turnewitsch et al. (2008) and procedures used for total ^{234}Th samples from the EMed were very similar to the ones used in the NEA. The analytical procedures used are similar to those outlined by Turnewitsch and Springer (2001) and largely follow Rutgers

van der Loeff and Moore (1999) and Rutgers van der Loeff et al. (2006). In the following we only give detailed descriptions of procedural steps that differ from the procedures outlined by Turnewitsch et al. (2008).

Consistently 8-L samples were processed. Because of the short duration of the cruise ^{234}Th samples were measured after the cruise in the shore-based lab at the University of Rostock. The radiation from the filter packages was measured non-destructively in a Risø GM25-5A beta multicounter. All samples were measured five times over 212–275 d to be able to investigate the shape of the decay curve for any contaminating radiation and to determine backgrounds caused by any beta emitters with half-lives much longer than the half-life of ^{234}Th. The time spans between sampling and the first measurements were 13–21 d.

Two batches of filters (F1 and F2) were used which differed in backgrounds and counting efficiencies. The average $\pm$1SD background counts were 0.37 ± 0.06 cpm ($N = 77$) and 1.04 ± 0.05 cpm ($N = 29$) for F1 and F2, respectively. The overall counting efficiency for F1 was determined by assuming radioactive ^{234}Th/^{238}U equilibrium for six replicate samples that were collected in the interior of the Rhodes Basin (Table 1), i.e., well away from any basin boundaries (at 2001 m water depth, 2428 m above the seafloor, ~50 km south of the Turkish continental slope at the sampling depth). For these six samples the average $\pm$1SD counting efficiency was 0.300 ± 0.007. This agrees within analytical uncertainties with the independently determined counting efficiency of 0.282 ± 0.014 of a set of standard filters carrying a known ^{238}U activity in equilibrium with ^{234}Th. The precision of the set of six interior Rhodes Basin samples was $\pm$1.9% (average $\pm$1SD: (2.75 ± 0.07) dpm L^{-1}). The average counting efficiency for F2 was determined to be 0.32 by using standard filters.

The ^{238}U activity in seawater was calculated based on ^{238}U–salinity relationships. In this study, we follow the relationship of Chen et al. (1986) for the NEA samples and the most up-to-date ^{238}U–salinity relationship for the Mediterranean as recommended by Pates and Muir (2007).

Total ^{234}Th activities were corrected for ^{234}Th ingrowth from ^{238}U during the analytical procedure. As the reported activities are expressed as activity per volume of seawater, activities were corrected for the pressure-related volume change between the in-situ sampling depth and the shipboard environment. All errors are reported as plus/minus one standard deviation ($\pm$1SD) and have been propagated considering uncertainties in pressure, temperature, salinity, density, difference among detectors, counts per minute (cpm), estimate of the activity at the time of sampling, counting efficiency, volume of filtered water and ^{238}U activity.

The total number of samples for the two study regions is roughly similar. However, the water-column samples in the NEA region were collected on a number of summer cruises between 1997 and 2005 (Turnewitsch et al., 2008), whereas the EMed samples were collected during a single 2-week 'snapshot' in December 2006. This difference may have resulted in not quantified uncertainties related to the potentially different impact of temporal variability on different time scales. This difference between the two sample sets needs to be kept in mind when the results are interpreted.

2.3.3. A subset of contaminated samples

Decay curves of several ^{234}Th samples showed peculiarly high activities during the first measurement indicating some form of short-lived contamination. The following samples were affected: CTD 892: 25, 40, 49, 60, 69 mab; CTD 893: 51, 60, 69 mab; CTD 907: 61, 71 mab; CTD 909: 767, 962, 1159 mab; CTD 935: 39, 49, 59 mab (Table A1). Except for CTD 909 these contaminations only occurred in samples from the bottommost ~100 m of the water column. We have no evidence for methodical problems and, therefore, think these contaminations originate from the sample material. Here we can only speculate about possible contaminants.

Rise, slope and summit sites on the Anaximenes Seamount were successfully sampled with a multiple corer demonstrating the presence of a sediment cover on the seamount. These sediments would provide a source for short-lived radium isotopes (^{223}Ra, ^{224}Ra) seeping from sediment pore waters and resulting in a radioactive excess of these nuclides in the near-bottom water column. Radium, if present, would have been precipitated together with thorium in the artificially formed MnO_2 particles that were used to extract the ^{234}Th from the water samples (see procedure described by Turnewitsch et al., 2008). ^{223}Ra and ^{224}Ra have half-lives of 11.43 and 3.66 d, respectively. Given a minimum time of 13 d between sampling and the first measurement most excess ^{224}Ra would have decayed by the time of the first measurement. ^{223}Ra, however, could still have been present contaminating the ^{234}Th signal for up to a maximum of ~60 d after sample collection. Both ^{223}Ra and ^{224}Ra are alpha emitters and would not be directly registered by the beta counter. However, further down their respective decay series there are only very short-lived daughters (half-lives <11 h), and both nuclides have daughter nuclides (^{223}Ra: ^{211}Pb, ^{207}Tl; ^{224}Ra: ^{212}Bi) that are beta emitters with maximum beta energies sufficiently high (^{211}Pb and ^{207}Tl: 1.4 MeV; ^{212}Bi: 2.3 MeV) to be registered by the beta counter (for comparison, ^{234}Th, whose maximum beta energy is 0.2 MeV, is effectively measured through its direct daughter ^{234}Pa with a maximum beta energy of 2.3 MeV).

Therefore, to estimate ^{234}Th activities in the contaminated samples the first measurement was omitted for the fit of the decay curve. This resulted in the time span between sampling and the first measurement that was used for the curve fitting to increase to 44–66 d (1.8–2.7 ^{234}Th half-lives). For the contaminated samples this inevitably led to unusually high analytical uncertainties of estimated ^{234}Th activities as can be seen in Table A1.

Given the half-life of ^{223}Ra of 11.43 d there could, in principle, still be contaminating radiation affecting measurements at $\geqslant$44 d after sampling. For the following two reasons we, however, think that in this case the effect of any ^{223}Ra remaining after 44 d is negligible. (1) After omission of the first measurement the quality of the curve fit was in the range of $r^2 = 0.9965$ up to $r^2 = 0.9999991$,

with 13 out of a total of 16 contaminated samples (81%) showing $r^2 > 0.999$. These excellent fits based on the ^{234}Th half-life of 24.1 d suggest that any remaining contamination was negligible after 44 d. (2) Moreover, as the half-life of ^{223}Ra is less than half the half-life of ^{234}Th any contaminating effect of ^{223}Ra decays more quickly than ^{234}Th. For example, at 44 d after sampling 28% of the original ^{234}Th are still left whereas only 7% of the original ^{223}Ra are left. That is, in relative terms the intensity of the contamination after 44 d is only $7/8 = 25\%$ of the original intensity of the contamination. The excellent curve fits demonstrate that also in absolute terms the contaminating effect should have been reduced to negligible levels at $\geqslant$44 d after sampling.

The samples of this study suggest that even in certain deep-sea environments there is the risk of sample contamination by beta emitters other than ^{234}Th and care is required to spot the affected samples. This is a methodological aspect that was already emphasized by Waples et al. (2003) for the measurement of ^{234}Th in freshwater systems.

The near-seafloor ^{234}Th samples that were collected in the abyssal NEA did not show any evidence of contamination (Turnewitsch and Springer, 2001; Turnewitsch et al., 2008). This is despite the fact that both NEA and EMed samples were collected near the Ra source of the seafloor. A possible reason for this difference lies in the tectonic activity of the EMed. The study area in the EMed is tectonically very active (e.g., ten Veen et al., 2004; Loncke et al., 2006) and known to comprise mud volcanoes and sites with active fluid seeps at the seafloor towards the east of the Anaximenes Seamount (e.g., Aloisi et al., 2004; Olu-Le Roy et al., 2004; Zitter et al., 2005; Haese et al., 2006). On the western side of Anaximenes, where our water-column samples were collected, the so-called Great Slide forms a huge north- and southwestward-flowing debris-flow unit (Fig. 1b) with evidence for gas venting or upward fluid release from the seafloor (ten Veen et al., 2004). In comparison to the tectonically inactive or much less active study region in the NEA such processes could increase the flux of short-lived Ra isotopes from the seafloor into the near-bottom water column at the Anaximenes Seamount, resulting in plumes of enhanced ^{223}Ra and ^{224}Ra activity, some of which we may have captured by ^{234}Th sampling.

2.3.4. Uncertainties of measured ^{234}Th activities

For this study, we used the following approach to calculate the 1SD uncertainty associated with the sample activity (expressed in counts per minute) estimated for the time of sample collection. For a given sample all background-corrected data, A, of the decay curve were first log-transformed ($\ln A$) resulting in a linearised form of the actual exponential relationship between A (plotted on the y-axis) and time, t, after sample collection (plotted on the x-axis). For this linearised relationship the y-axis intercept, Y, and the values for Y+1SD and $Y-1$SD were estimated by a linear regression analysis. The actual sample activity at the time of sample collection, A_0, was then calculated by $A_0 = e^Y$. In the aforementioned linearised relationship between $\ln A$ and t the absolute values of +1SD and −1SD are identical. However, what we are interested in is not 1SD of the linearised relationship between $\ln A$ and t but the uncertainty of the y-axis intercept of the exponential relationship between A and t. This requires taking the antilog of Y, (Y+1SD) and ($Y-1$SD) which results in the values e^Y, $e^{(Y+1SD)}$ and $e^{(Y-1SD)}$. While $|Y-(Y+1SD)| = Y-(Y-1SD)$, however, $|e^Y - e^{(Y+1SD)}| > e^Y - e^{(Y-1SD)}$. That is, in the exponential relationship between A and t the upper (positive) part of the uncertainty of A_0 is higher than the lower (negative) part of its uncertainty. For each sample we, therefore, need to run two error propagations and report two uncertainty estimates: one upper (positive) and one lower (negative) one (Table A1).

We will see that in the EMed data set total ^{234}Th activities scattered around the ^{238}U activity and in only 7% of the samples was there a detectable disequilibrium between total ^{234}Th and ^{238}U. It seems, however, that total ^{234}Th activities were typically slightly greater than the equilibrium value. Perhaps either the ^{234}Th activities are being overestimated or the ^{238}U activities are being underestimated. At this stage we have no information that would allow us to pinpoint the reason for this phenomenon. This phenomenon and the uncertainties have no impact on the main outcome of this study.

2.4. Particulate organic carbon (POC) and nitrogen (PON)

At the Anaximenes seamount water samples for POC and PON analyses were collected. The procedures for the determination of POC and PON concentrations were based on Verardo et al. (1990) and Turnewitsch et al. (2007). For each sample 8 L of water were filtered at a vacuum of ~300 mbar through pre-combusted (500 °C for 12 h) and pre-weighed 25 mm-diameter Whatman GF/F-filters. Until analysis the filters were stored deep-frozen and individually in small plastic Petri-dishes covered by a lid. Before further analysis the filters were dried at 60 °C for 12 h and weighed. In order to remove carbonates the filters were kept in fumes of hydrochloric acid (37% w/w) for 12 h, rinsed with Milli-Q water, dried again and weighed. Unused pre-combusted GF/F-filters (blank filters) were treated in the same way. For the measurement of POC and PON the filters were folded in aluminium foil and measured in a Carlo-Erba CHN-Analyzer largely following (Verardo et al., 1990). The CHN analyser was calibrated with acetanilide and blank values for the calibration were determined with empty aluminium capsules.

There is growing evidence that adsorption of dissolved organic material (DOM) onto GF/F-filters biases estimates of POC and PON concentrations if data are not corrected for this adsorption (Menzel, 1966; Moran et al., 1999; Gardner et al., 2003; Liu et al., 2005; Turnewitsch et al., 2007). To assess the effect of DOM adsorption onto filters an experiment was run to estimate the amount of organic carbon (OC) and nitrogen (ON) adsorbed to the filters. Different volumes (0.1, 0.2, 0.5, 1, 2, 5 and 10 L) of mid-depth water from the Rhodes Basin (from 2001 m depth, 2428 m above the seafloor, i.e., the same water parcel as

sampled for the determination of the counting efficiency of the beta counter) were filtered on the same filtration device. Measured OC and ON contents on the filters (Table A2) (plotted on the y-axis) were related to the filtered volume (plotted on the x-axis) and a linear regression was accomplished. The relationships for organic carbon and nitrogen were $M_{OC} = 0.0131 \times V + 0.058$ ($r^2 = 0.7433$) and $M_{ON} = 0.0006 \times V + 0.0021$ ($r^2 = 0.9575$), respectively, where M_{OC} (in mg) and M_{ON} (in mg) are the total masses of OC and ON on the filter and V (in L) is the filtered volume. The resulting y-axis intercepts (measures for the amount of adsorbed material: 0.058 mg OC per filter = 5 μmol OC per filter = 1.2 μmol OC cm^{-2} of exposed filter area; 0.0021 mg ON per filter = 0.15 μmol ON per filter = 0.036 μmol ON cm^{-2} of exposed filter area) were subtracted from the total OC and ON amounts on each sample filter.

Given the fact that the samples were obtained from a deep-sea environment there is unusually large scatter in the M_{OC}–V relationship (cf. Fig. 1 in Turnewitsch et al., 2007), and the estimated amount of adsorbed OC is unusually large (cf. Table 2 in Turnewitsch et al., 2007). By contrast, the M_{ON}–V relationship is of good quality and the estimated amount of adsorbed ON is very similar to the corresponding value for the deep open Northeast Atlantic (cf. Turnewitsch et al., 2007). We do not know the reason for the poor quality and high y-axis intercept of the M_{OC}–V relationship but one possibility is OC that was low in ON and leached from the acid-cleaned but brand new collapsible plastic containers used.

It has been shown that DOM adsorption may not be the only phenomenon affecting the determination of absolute POC and PON concentrations (Liu et al., 2005; Turnewitsch et al., 2007). In this study, all samples were obtained from the deep water column (depths >600 m). This should rule out any significant impact on concentration estimates of differences of methodological biases between surface- and deep-ocean samples (cf. Turnewitsch et al., 2007). Moreover, we are only interested in the relative differences between samples rather than absolute concentrations. For the purposes of this study it, therefore, seems possible to use the adsorption-corrected POC and PON concentration estimates even if their absolute values might be biased by processes other than DOM adsorption onto the filters (e.g., artificial formation of filterable particles during processing of bottle samples).

3. Results

3.1. Flow dynamics

Results for the NEA study region had already been discussed by Turnewitsch et al. (2008). Our knowledge is based on published information on water-mass distribution and current velocities (Dickson et al., 1985; Mittelstaedt et al., 1986; Klein and Mittelstaedt, 1992; McCartney, 1992; Lampitt et al., 2001; Vangriesheim et al., 2001), Regional Ocean Model System (ROMS) modelling of the flow field resulting from residual flow impinging on a short seamount (Turnewitsch et al., 2004), and modelling and geographical mapping of barotropic (Egbert and Erofeeva, 2002) and baroclinic M_2 tides (Nycander, 2005; Turnewitsch et al., 2008).

To facilitate the comparison of the NEA and the EMed we briefly summarise the key NEA facts here. Total current velocities at the PAP site were almost always $<15\,cm\,s^{-1}$, and residual flow was typically ~4–5 $cm\,s^{-1}$ (Lampitt et al., 2001; Vangriesheim et al., 2001). Semi-diurnal tides are superimposed on this residual flow (Vangriesheim et al., 2001) with the maximum barotropic spring tide current velocities being ~5 $cm\,s^{-1}$. At the BIOTRANS site the flow is strongly influenced by the seafloor topography (Mittelstaedt et al., 1986). The typical range of average horizontal current velocities was 1–4 $cm\,s^{-1}$. Energy spectra of the currents show a pronounced peak for the semi-diurnal tide with tidal current velocities up to 6 $cm\,s^{-1}$ near sloping seafloor during spring tide. Near topography (particularly on (near-)critical slopes) internal tides increase the tidal component of the flow by a factor of ~2 (Turnewitsch et al., 2008). In a number of locations in the NEA study region tides push total current velocities above the estimated threshold for sediment erosion or resuspension (~(6.5–10.5)$cm\,s^{-1}$).

The basin-wide near-surface circulation in the EMed is composed of a complex combination of large-scale currents and a system of quasi-permanent meso-scale gyres and transient eddies (see Fig. 3 and Robinson et al. (1991) for a detailed summary). An 8-week average (November 2006–January 2007) of dynamic topography (cm) and geostrophic currents ($cm\,s^{-1}$) calculated from the weekly composites of AVISO satellite altimetry described in Section 2.2 is shown in Fig. 3a. The Anaximenes seamount is located between the eastward Mid-Mediterranean Jet (MMJ) to the south and the westward Asia Minor Current (AMC) to the north at the eastern rim of the Rhodes cyclonic gyre. Meso-scale variability in the vicinity of Anaximenes Seamount was generally low for the sampling period (Fig. 3b). Enhanced levels of variability were apparent in Turkish coastal areas and south of Cyprus but did not penetrate the seamount region. AVISO-determined surface currents at the seamount were mainly to the northwest with an average velocity of 15 $cm\,s^{-1}$.

These values were generally in good agreement with near-surface values obtained from the ship-board ADCP recordings. ADCP currents at the Anaximenes sampling locations were averaged over each individual sampling period and, therefore, represent a combination of long-term residual flow and short-term variability patterns. Surface currents varied between 6 and 12 $cm\,s^{-1}$, predominantly westward (Fig. 4). Flow characteristics significantly changed in the deeper layers with a tendency to eastward flow superimposed by occasional flow reversals in the 100–400 m depth interval. Corresponding velocities dropped sharply to absolute values not exceeding 5 cm s^{-1}. Long-range ADCP recordings down to seamount summit depths (approximately 750 m) were available for the last four stations and showed consistently low current velocities of approximately 3–4 $cm\,s^{-1}$ at depths greater than 400 m. Flow variability at these depths appeared to

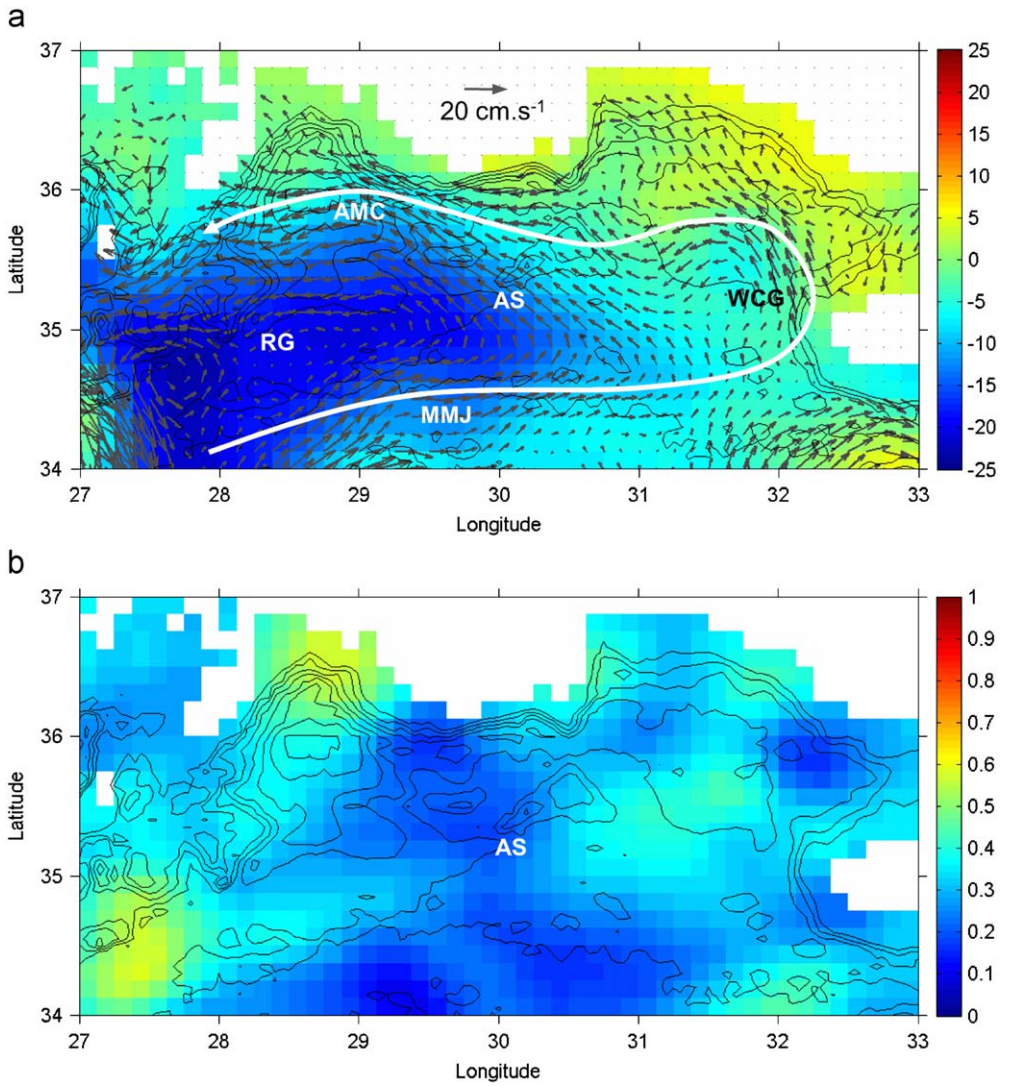

Fig. 3. (a) Eight weeks average (November 2006–January 2007) of weekly AVISO composites of absolute dynamic topography (cm) and geostrophic velocity (cm s^{-1}). Anaximenes Seamount (AS), Rhodes Gyre (RG), West Cyprus Gyre (WCG), Mid-Mediterranean Jet (MMJ), Asia Minor Current (AMC). (b) Normalized standard deviation of absolute dynamic topography.

be dominated by an oscillatory pattern in northwest–southeast directions.

In the absence of deep in-situ current measurements barotropic tidal characteristics predicted by the OSU inverse tidal model (Egbert and Erofeeva, 2002) were analysed to evaluate the potential of Anaximenes seamount as a region of locally amplified flow in response to oscillatory forcing. The tidal current ellipses for the dominant semi-diurnal (M_2) and diurnal (K_1) tidal constituents in the vicinity of the seamount for December 2006 as derived from the OSU tidal model are shown in Fig. 5. Barotropic tidal flow in the far field off the seamount was uniformly orientated in the east–west direction. Semi-diurnal and diurnal barotropic tidal currents were very weak with typical velocities of 3.5 and 0.5 mm s^{-1}, respectively. Maximum barotropic tidal current velocities during spring tide were ~5 mm s^{-1} (Fig. 2). The lowest barotropic tidal current velocities were predicted for the start of the cruise during neap tide, the highest velocities at the end during spring tide. There was some moderate modulation of diurnal tidal currents in the slope regions of the seamount showing more circular current ellipses and cross-slope tidal flow. Because of the resolution of the OSU Mediterranean tidal solution (1/12°), missing detail of the model bathymetry may result in a slight underestimation of tidal current amplitudes. However, the analysis of tidal characteristics provided two major results: (i) semi-diurnal barotropic tidal currents generally exceeded peak values of diurnal tidal currents by one order of magnitude and (ii) there was no apparent amplification of diurnal tidal currents at the seamount slope compared to the immediate far field.

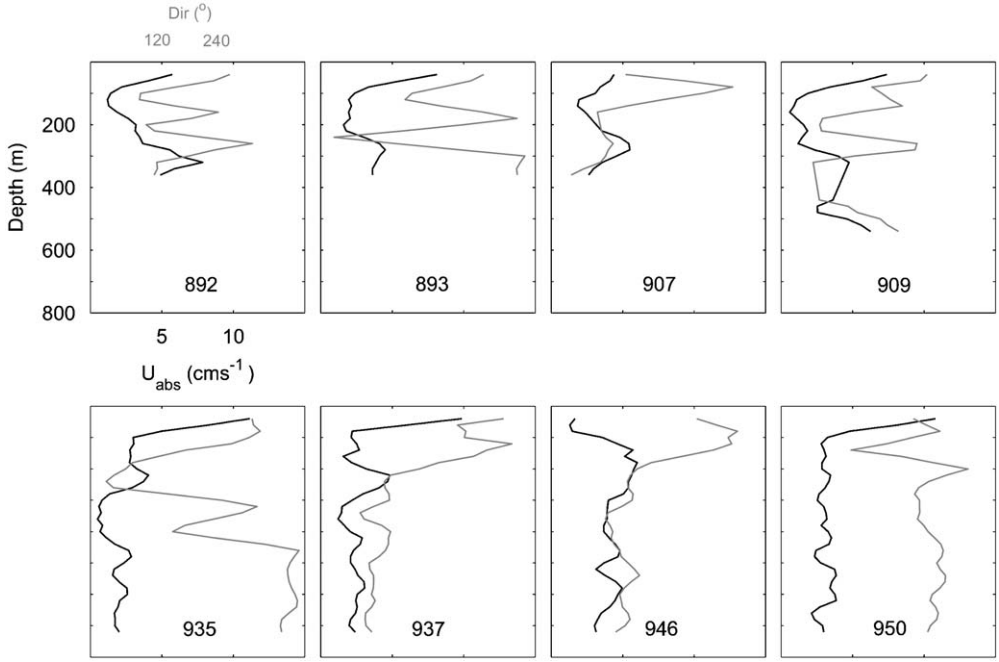

Fig. 4. Vertical profiles of horizontal current velocities (cm s^{-1}) and directions (deg) as obtained from the ship-board ADCP, averaged over each water-column sampling location (see Table 1 for station locations and sampling times). The depth scale for the upper left figure also applies to all other figures. Eastward and westward currents are indicated by 90° and 270°, respectively.

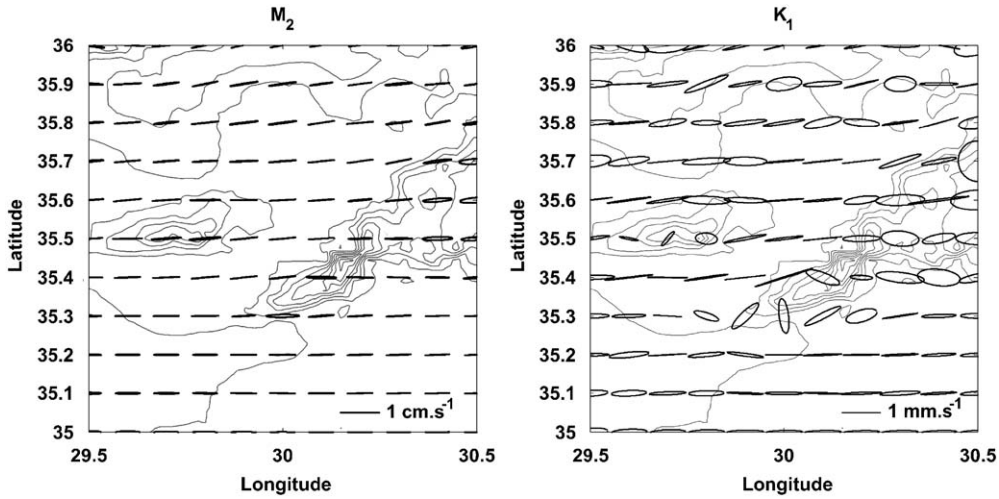

Fig. 5. Current velocity ellipses for M_2 and K_1 tidal constituents for December 2006 from the OSU Mediterranean Sea regional tidal model solution (Egbert and Erofeeva, 2002).

3.2. *Water-column distribution of ^{238}U, total ^{234}Th, and POC and PON*

Thorium-234 and ^{238}U results for the NEA study region have already been presented and discussed by Turnewitsch et al. (2008). The sampling sites were downstream of, or surrounded by, fields of short seamounts. At the sampling sites between about 200 and 1000 m above the seafloor recurrent 'fossil' disequilibria were observed. We define 'fossil' disequilibria as clearly detectable ^{234}Th/^{238}U disequilibria in combination with low particle-associated ^{234}Th activities. 'Fossil' disequilibria were centered at levels in the water column that correspond to the average height of the short seamounts near the sampling sites. This suggests the 'fossil' disequilibria are formed on the seamount slopes. The vertical distribution of light transmission at the PAP site (Turnewitsch and Springer, 2001) supports this notion (Turnewitsch et al., 2008). A summary of the vertical

overall distribution of total ^{234}Th relative to ^{238}U in the NEA study region is shown in Fig. 6a.

At the Anaximenes seamount sites the average total ^{234}Th of the whole data set is 2.82 dpm L^{-1} (black diamond in Fig. 6b) with individual activities ranging from 2.45 up to 3.17 dpm L^{-1}. Upper and lower average $\pm$1SD uncertainties are 0.27 $\pm$ 0.20 and 0.24 $\pm$ 0.16 dpm L^{-1}, respectively (error bars associated with the black diamond in Fig. 6b); the corresponding ranges for upper and lower uncertainties of the individual activities are 0.05–0.92 and 0.05–0.68 dpm L^{-1} (Table A1). The average $\pm$1SD salinity-derived ^{238}U activity was 2.74 $\pm$ 0.01 dpm L^{-1} (according to Pates and Muir (2007) the actual uncertainty of individual ^{238}U activities is $\sim\pm$2% though). Using $\pm$1SD as an estimate for overall uncertainties it can be concluded that 93% of all total ^{234}Th samples from the EMed study were in radioactive equilibrium with ^{238}U. Only 7% of the sample set had detectable disequilibria and there was no spatial or temporal pattern or trend in the occurrence of these rare disequilibria (Fig. 6b and Tables 2 and A1). It can, therefore, be concluded that total ^{234}Th on the western side of the Anaximenes seamount was almost always in radioactive equilibrium with its parent ^{238}U during the sampling interval (14–21 December 2006) and throughout the sampled water column (754–2107 m depth; estimated 7–1175 mab).

In the EMed POC and PON distributions were largely homogeneous in the sampled water column. There was no clear and reproducible evidence for increased concentrations in the near-bottom water column, and there was no evidence for intermediate nepheloid layers (Table A3). Overall, mean $\pm$1SD POC concentrations (per CTD deployment) in the upper water column (samples from 100 to 1200 mab) were between $\sim$5 $\pm$ 6 and $\sim$10 $\pm$ 5 μg L^{-1} and in the BBL (samples from 10 to 50 mab) between $\sim$5 $\pm$ 2 and

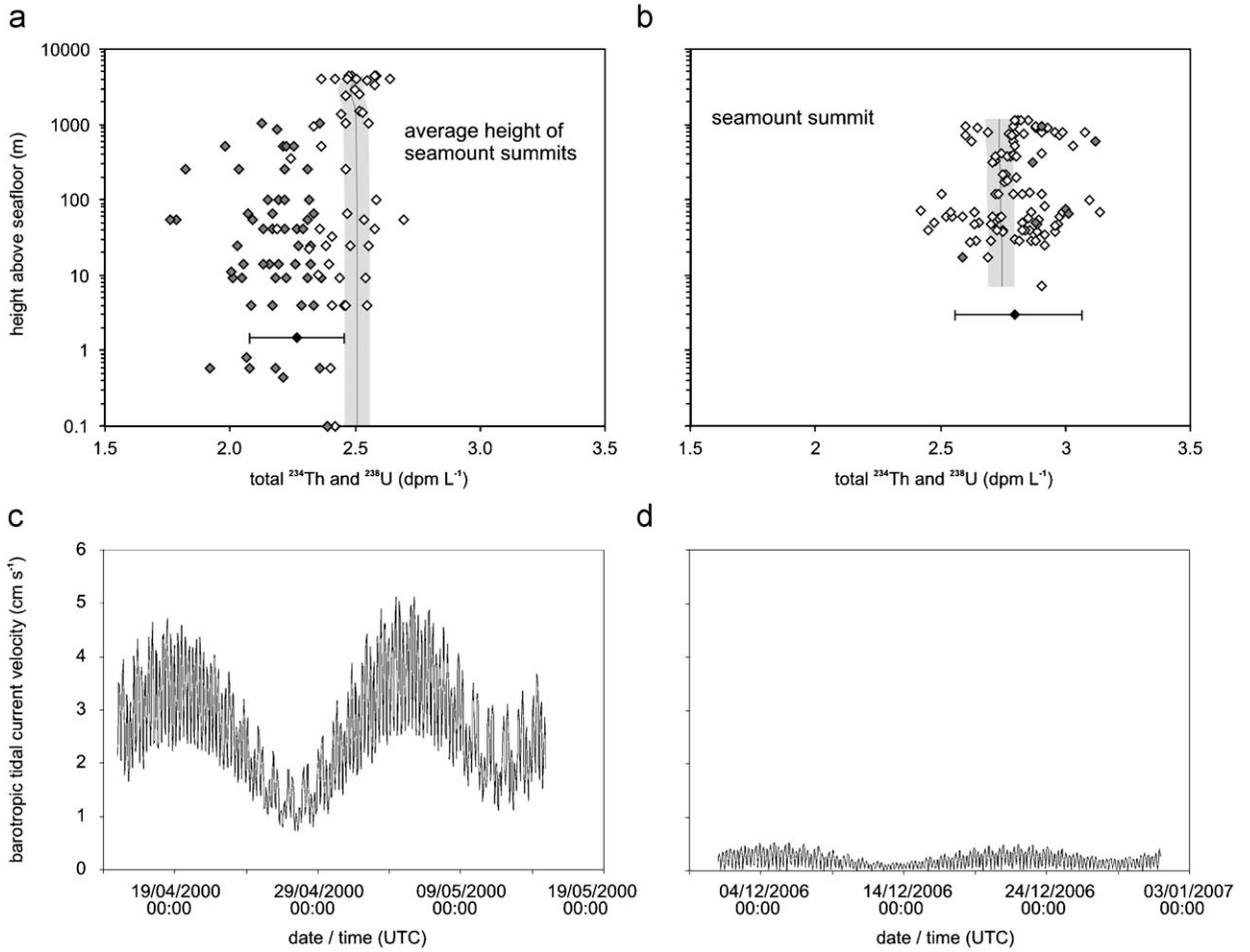

Fig. 6. Comparison of total ^{234}Th/^{238}U disequilibria (a, b) and barotropic tidal current velocities (c, d) between the deep-sea environments of the Northeast Atlantic (a, c) and the Eastern Mediterranean (b, d). The Northeast Atlantic data are taken from Turnewitsch et al. (2008). Black lines in (a, b): ^{238}U activities calculated from salinity according to Chen et al. (1986) for the NEA data and Pates and Muir (2007) for the EMed data. Grey range behind black ^{238}U lines: 1SD uncertainty of ^{238}U activities based on Pates and Muir (2007). Black diamonds with error bars in (a, b): (a) mean $\pm$1SD of the samples from within the bottommost 1000 m of the water column of the NEA study region and (b) the mean $\pm$1SD of all samples from the EMed study region. Grey diamonds indicate samples with detectable radioactive disequilibria between total ^{234}Th and ^{238}U.

$\sim 16 \pm 2\,\mu g\,L^{-1}$. Overall, corresponding mean PON concentrations in the upper water column were between 0.33 ± 0.03 and $1.0 \pm 0.9\,\mu g\,L^{-1}$ and mean values in the BBL between 0.36 ± 0.08 and $1.0 \pm 0.3\,\mu g\,L^{-1}$. Neither POC nor PON concentrations showed any clear differences between neap and spring tides (Table A3).

4. Discussion

The principal goal of this study was to investigate whether there is any difference in the water-column distribution of the naturally occurring short-lived particulate-matter tracer ^{234}Th between two deep-sea environments with different tidal forcing. The motivation for this study is the requirement for an improved understanding of how tidal fluid dynamics are reflected in sediment-geochemical parameters that may help pave the way to a new approach for the reconstruction of past fluid dynamics in the deep ocean.

4.1. Comparison of the physical conditions at the study sites

For the comparison of the study region with typical deep open-ocean tides (NEA) and the study region with very weak tides (EMed) a number of parameters need to be considered: Froude number; Coriolis parameter (geographical latitude); predominant tidal frequency; buoyancy frequency (a measure for the intensity of the density stratification of the water column); the resulting wave characteristic of the internal tide (the angle at which rays of internal waves of tidal frequency propagate); the slope criticality which is controlled by the seamount geometry (specifically the slope angle) relative to the wave characteristic; and current velocities and prevailing directions of residual flow, barotropic tidal flow, and baroclinic tidal flow. The comparison between the NEA and EMed study regions is summarised in Table 2.

One requirement for the occurrence of internal tides in the deep ocean is that the horizontal scale of the topography, k^{-1}, exceeds the tidal excursion scale U_0/ω_0, i.e., $kU_0/\omega_0 \ll 1$. For $Fr \geqslant 1$ the likeliness of the occurrence of internal lee waves in addition to, or instead of, internal tides increases. Given $k^{-1} \approx O(1\text{–}10$ km) and $\omega_0 = 1.454 \times 10^{-4}\,s^{-1}$ in both study environments, and given $U_0 \approx 1.4\,cm\,s^{-1}$ in the NEA study region and $U_0 \approx 0.25\,cm\,s^{-1}$ in the EMed study region (Fig. 6c and d) it can be concluded that $Fr \ll 1$ in both study environments and that baroclinic tides, rather than lee waves, are formed.

The Coriolis parameter, f, predominant tidal frequency and buoyancy frequency are all similar in both study regions. In the NEA region f is only $\sim$1.24–1.29 times higher than at the EMed site, and the predominant tidal frequency is semi-diurnal ($1.454 \times 10^{-4}\,s^{-1}$) in both environments. The buoyancy frequency in the water column of the deep NEA is $\sim 8 \times 10^{-4}\,s^{-1}$ and largely invariant (unpublished data; van Haren, 2007) whereas in the sampled layer of the water column in the Mediterranean it was $\sim 7 \times 10^{-4}\,s^{-1}$.

A key parameter for the determination of the magnitude of the likely impact of internal tide formation on

Table 2
Comparison of the Northeast Atlantic and Eastern Mediterranean study regions.

	Northeast Atlantic	Eastern Mediterranean
Total ^{234}Th/^{238}U disequilibria near topography	In 59% of all samples; no detectable ^{234}Th/^{238}U activity ratios >1	In 7% of all samples; some of the few detectable ^{234}Th/^{238}U activity ratios >1
Froude number $= kU_0/\omega_0$	$\ll 1$	$\ll 1$
Coriolis parameter, f (s^{-1})	1.066×10^{-4}–1.103×10^{-4}	0.857×10^{-4}
Predominant tidal frequency, ω_0 (s^{-1})	1.454×10^{-4} (semi-diurnal)	1.454×10^{-4} (semi-diurnal)
Buoyancy frequency, N (s^{-1})	8×10^{-4}	7×10^{-4}
Wave characteristic: $s = ((\omega_0^2 - f^2)/(N^2 - \omega_0^2))^{0.5}$	0.12–0.13	0.17
(Near-)critical slope angles	Yes: on slopes of a number of nearby seamounts	Yes: certain sections on the slope of the seamount
Residual far-field flow ($cm\,s^{-1}$)	4–5 (mainly northward directions)	$\sim <4$ (no direct information on prevailing direction for deeper water column)
Barotropic tides	Typical open-ocean current velocities: maximum during spring tide $\sim 5\,cm\,s^{-1}$; orientation of tidal ellipse similar to prevailing northward residual flow	Very weak: maximum during spring tide $\sim 0.5\,cm\,s^{-1}$; very predominant E–W components
Baroclinic tides	Model-derived evidence for baroclinic tides locally increasing total tidal current velocities by a factor of ~ 2	No direct evidence for the effect of baroclinic tides; given weak barotropic tides the effect of baroclinic tides on current velocities cannot be high though
Total current velocities relative to critical current velocities for sediment erosion/resuspension	Total maximum current velocities locally $\sim 15\,cm\,s^{-1}$, i.e., $>$critical velocity (~ 6.5–$10.5\,cm\,s^{-1}$)	Total maximum current velocity estimated to be $\sim 5\,cm\,s^{-1}$, i.e., $<$critical velocity (~ 6.5–$10.5\,cm\,s^{-1}$)
Seamount height relative to nearby plain	Average ~ 600 m (maximum ~ 1100 m)	Maximum ~ 1300 m
Seamount shape	Numerous seamounts with very varied shapes and orientations relative to the tidal current vector ellipse and residual flow	Elongated at approximately 45° to the tidal current vector ellipse

sediment erosion and resuspension is the so-called slope criticality. As already mentioned in the Introduction (near-)critical slope sections are associated with the formation of internal tides, particularly intense fluid dynamics and locally increased current velocities near the seafloor. These slope sites are, therefore, most likely to influence sediment dynamics. In the NEA region C ranges between ~0 and ~2.5. Vast areas have $C<0.5$, but (near-)critical slopes occur on a number of short seamounts which are very likely to influence the ^{234}Th distribution in this environment (Turnewitsch et al., 2008). On the western side of the Anaximenes Seamount (near-)critical slope sections also occur. We can, therefore, conclude that both deep-sea environments contain (near-)critical topographic slopes where internal tides are likely to be formed.

The presence of potential formation sites of internal tides in itself is not sufficient to also imply the probability of sediment erosion and resuspension. The internal tide has also to be sufficiently strong to increase the local current velocity near the seafloor above the critical threshold for sediment erosion and resuspension. This threshold has been estimated to be ~6.5–10.5 cm s^{-1} for the fluffy, aggregated particulate matter (Lampitt, 1985; Ziervogel and Bohling, 2003; Turnewitsch et al., 2008) that can be found to form the topmost sediment layer in many deep-sea environments. This fluffy, aggregated material is believed to be the main subject of sediment erosion and resuspension (Lampitt, 1985; Walsh et al., 1988; Walsh, 1992) and has been observed in the NEA study region as well as in the EMed study region.

To estimate whether total current velocities could have become sufficiently high to erode and resuspend surface sediments, information on barotropic plus baroclinic tidal flow and residual flow is required. For the NEA region these flow velocities are reasonably well constrained (Lampitt et al., 2001; Vangriesheim et al., 2001; Turnewitsch et al., 2004, 2008). As already mentioned in Section 3.1 the residual flow is ~4–5 cm s^{-1} and barotropic tidal maximum current velocities during spring tide are ~5 cm s^{-1}. Baroclinic tides locally increase the tidal current velocity near the seafloor by a factor of ~2 (Turnewitsch et al., 2008). A simple linear addition of barotropic tidal, baroclinic tidal and residual current velocities results in an estimate of the maximum total current velocity of ~15 cm s^{-1} (Turnewitsch et al., 2008). Here this linear addition is applicable as the orientation of the tidal current vector ellipse is very similar to the prevailing northward direction of the residual flow. The maximum estimate corresponds well to the measured data presented by Lampitt et al. (2001), which show that current velocities at about 150 m above bottom in the Porcupine Abyssal Plain are almost always ~≤15 cm s^{-1}. It can be concluded (see Turnewitsch et al., 2008) that in the NEA region tides, in particular baroclinic tides, locally push the total current velocities near the seafloor above the threshold for sediment erosion and resuspension of ~6.5–10.5 cm s^{-1}.

Residual current velocities at the Anaximenes Seamount are not as well constrained as in the NEA region. However, we believe we have sufficient information to be able to compare the situation at the Anaximenes Seamount with the situation in the NEA. We have no direct observations of residual current velocities in the deep water column of the EMed that was sampled for ^{234}Th. The geographical distance between the two sampling sites (~2.5 km) was too small and the sampling sites were too close to the topography to calculate current velocities based on the geostrophic method. However, Aviso modelling and ship-based ADCP measurements showed that residual current velocities decreased from 8 to 15 cm s^{-1} in the surface water column to ~3–4 cm s^{-1} at 750 m depth. It, therefore, seems reasonable to assume that residual current velocities in the far field away from the seamount tended to be ≤4 cm s^{-1}, a value very similar to that of the NEA study region (Table 2).

At the Anaximenes seamount maximum barotropic tidal current velocities were found to be 4 mm s^{-1} (M_2, semi-diurnal), 2.2 mm s^{-1} (S_2, semi-diurnal), 0.7 mm s^{-1} (K_1, diurnal) and 0.4 mm s^{-1} (O_1, diurnal). Overall maximum barotropic tidal current velocities during spring tide at the Anaximenes Seamount were only ~0.5 cm s^{-1} during the observation period (Fig. 2). In comparison, typical tidal amplitudes on the Porcupine Abyssal Plain in the NEA region are on the order of 3.5 cm s^{-1} (M_2), 1.4 cm s^{-1} (S_2), 0.3 cm s^{-1} (K_1) and 0.18 cm s^{-1} (O_1). The overall maximum barotropic tidal current velocities during spring tide were on the order of ~5 cm s^{-1}, generally one order of magnitude higher than in the EMed (Fig. 6).

We have no direct information on baroclinic tides in the EMed study region. Based on the work of Turnewitsch et al. (2008) and more idealised model studies of internal tide formation (e.g., Balmforth et al., 2002; Llewellyn Smith and Young, 2002; Khatiwala, 2003; Legg and Huijts, 2006) it seems reasonable to assume that baroclinic tides increase total tidal current velocities by a factor of ~2. Given the occurrence of (near-)critical slopes on the Anaximenes seamount baroclinic tides are probably formed. Given the extremely small maximum current velocities of the barotropic tide, however, these baroclinic tides are unlikely to be higher than ~0.5 cm s^{-1}. Residual, barotropic tidal and baroclinic tidal flow could, therefore, add up to a maximum total current velocity of ~5 cm s^{-1}. This is lower than the estimated critical threshold current velocity of ~6.5–10.5 cm s^{-1} for sediment erosion/resuspension.

As mentioned above, asymmetric flow fields surrounding kilometer-scale seafloor elevations of comparable breadth and width may support locally amplified residual current velocities that can lead to locally enhanced sediment erosion and resuspension. We cannot rule out that this phenomenon becomes relevant on certain parts of the Anaximenes seamount.

4.2. The importance of tides for sediment dynamics in the deep sea

The above discussion shows that in almost all relevant fluid-dynamical aspects the NEA and EMed study regions

are rather similar. The only major difference seems to be the tidal forcing, with maximum barotropic tidal current velocities in the NEA being about one order of magnitude higher than in the EMed. Based on the information compiled in Table 2 it can be concluded that, in contrast to the NEA study region, barotropic and baroclinic tides in the EMed are very unlikely to be strong enough to push total current velocities above the threshold for sediment erosion and resuspension.

In the following, we address the question whether this difference in tidal forcing is reflected in the water-column distribution of the naturally occurring short-lived particulate-matter tracer ^{234}Th. At the Anaximenes seamount total ^{234}Th was measured at two sites that were only about 2.5 km apart, one on the lower northwestern slope and another one just off the rise of the northwestern slope. There was no detectable difference between these two sites. Moreover, total ^{234}Th activities scattered around the ^{238}U activity and in only 7% of the samples was there a detectable disequilibrium between total ^{234}Th and ^{238}U (Fig. 6b).

Therefore, the total ^{234}Th distribution showed hardly any evidence for sediment erosion and resuspension in the water column on the northwestern side of the Anaximenes Seamount between 754 and 2107 m depth (7 and 1175 mab) on the characteristic time scale of ^{234}Th of up to a few weeks. This is despite the close proximity [O(1 km)] of the sampling sites to the seamount. The notion of weak or lacking sediment erosion and resuspension at the Anaximenes seamount is supported by the absence of a clear and consistent increase of the concentrations of POC and PON in the near-bottom water column, a distributional feature one would expect in areas of enhanced sediment resuspension. There was also no clear evidence for intermediate nepheloid layers.

The situation differs markedly in the NEA study region (Turnewitsch et al., 2008). In 59% of the samples from the bottommost ~1000 m of the water column disequilibria were detected. This includes recently formed disequilibria in the bottommost ~100 m and 'fossil' disequilibria higher up in the water column both of which are very likely to be formed and maintained by tidal forcing (Turnewitsch et al., 2008).

It can be concluded that the two main differences between the NEA and EMed study regions are the tidal forcing and the shape of the vertical distribution of ^{234}Th in the deep water column. It can, therefore, be suggested that the main reason for the difference in ^{234}Th distribution is the difference in tidal forcing. This study is additional support for the notion (Lampitt, 1985; Vangriesheim et al., 2001; Turnewitsch et al., 2008) that tides, and in particular internal tides (Turnewitsch et al., 2008), are of more importance for sediment dynamics in the deep sea away from continental slopes than previously thought.

5. Conclusions

This study provides further indirect evidence for the potential impact open-ocean tides may have on the erosion and resuspension of deep-sea sediments. Together with the work of Turnewitsch et al. (2004) on asymmetric flow fields and Turnewitsch et al. (2008) on internal tides and their impacts on sediment dynamics it also suggests that sedimentary records of deep-sea seamounts could have recorded past changes of residual flow and tidal forcing in the deep sea.

As tides and asymmetric residual flow can push total current velocities above the erosion and resuspension threshold distributional patterns of erosivity proxies in the sediment cover of deep-sea seamounts could archive the information on past changes of fluid dynamics. Promising proxies for sediment erosivity are distributions of grains sizes, heavy minerals and longer-lived particle-reactive radionuclides (e.g., Turnewitsch et al., 2004; McCave and Hall, 2006; Kienast et al., 2007).

Given model-derived evidence for significant paleochanges of tidal kinetic energy and tidal-energy dissipation in the deep sea over glacial/interglacial cycles (Egbert et al., 2004) the potential importance of deep-ocean tides for the formation and interpretation of sedimentary records in particular warrants further research. Tidal energy seems to be one of the major energy sources for the vertical mixing of the ocean (Wunsch and Ferrari, 2004) and the link between changing ocean overturning and changing tidally related ocean mixing is of great potential importance but remains unclear (Nilsson et al., 2003; Montenegro et al., 2007).

A better understanding of how tidal and residual flow dynamics are reflected in topographically controlled sedimentary records could help establish a sediment proxy for the reconstruction of past changes of key aspects of fluid dynamics in the deep open ocean. This study is one further piece of evidence that suggests the establishment of such a proxy could be possible.

Acknowledgements

We thank officers and crew of R.V. *Meteor* for their support and Johan H. ten Veen for providing the bathymetric data of the study region in the Eastern Mediterranean. Three anonymous referees provided very constructive and insightful comments which improved the manuscript. Funding by the Deutsche Forschungsgemeinschaft (DFG GR 816/5-1) is gratefully acknowledged. Additional support was provided by a grant (agreement no. ST/05/17) from the Marine Institute of Ireland and the Irish Marine RDTI Measure, Productive Sector Operational Programme, National Development Plan 2000–2006.

Appendix A

Compilations of sampling depths and heights above the seafloor and of radionuclide, POC and PON data are given in Tables A1–A3.

Table A1
Compilation of sampling depths and heights above the seafloor, ^{238}U and total ^{234}Th activities plus uncertainties.

Station ID	Total ^{234}Th (dpm L^{-1})	+1SD (dpm L^{-1})	−1SD (dpm L^{-1})	^{238}U (dpm L^{-1})	1SD (dpm L^{-1})	Depth (m)	Height above seafloor (m)
Rhodes Basin	2.75	0.08	0.08	2.75	0.05	2001	2428
CTD 881	2.64	0.07	0.06	2.75	0.05	2001	2428
	2.79	0.08	0.08	2.75	0.05	2001	2428
	2.68	0.08	0.07	2.75	0.05	2001	2428
	2.79	0.34	0.30	2.75	0.05	2001	2428
	2.81	0.13	0.12	2.75	0.05	2001	2428
Slope	2.93	0.18	0.17	2.73	0.05	964	807
CTD 892	3.15	0.22	0.21	2.74	0.05	1159	612
	2.77	0.13	0.13	2.74	0.05	1355	416
	2.79	0.16	0.15	2.74	0.05	1551	220
	2.94	0.13	0.12	2.74	0.05	1650	121
	2.67[a]	0.17	0.16	2.74	0.05	1702	69
	2.62[a]	0.78	0.60	2.74	0.05	1711	60
	2.86[a]	0.09	0.08	2.74	0.05	1722	49
	2.48[a]	0.92	0.68	2.74	0.05	1731	40
	2.94[a]	0.15	0.14	2.74	0.05	1742	25
Slope	2.99	0.44	0.38	2.73	0.05	967	804
CTD 893	2.65	0.14	0.13	2.74	0.05	1160	611
	2.93	0.50	0.43	2.74	0.05	1359	412
	2.78	0.29	0.26	2.74	0.05	1554	217
	2.75	0.08	0.07	2.74	0.05	1651	120
	2.66[a]	0.19	0.18	2.74	0.05	1702	69
	2.55[a]	0.63	0.51	2.74	0.05	1711	60
	2.68[a]	0.37	0.32	2.74	0.05	1720	51
	2.78	0.65	0.53	2.74	0.05	1731	40
	2.67	0.28	0.25	2.74	0.05	1742	29
Trough	2.84[b]	0.06	0.06	2.73	0.05	965	1160
CTD 907	2.63[b]	0.13	0.13	2.74	0.05	1161	964
	2.80[b]	0.21	0.19	2.74	0.05	1357	768
	2.81[b]	0.11	0.11	2.75	0.05	1752	373
	2.78	0.08	0.07	2.75	0.05	1948	177
	2.94[b]	0.14	0.13	2.75	0.06	2044	81
	2.45[a]	0.85	0.64	2.75	0.06	2054	71
	2.58[a]	0.16	0.15	2.75	0.06	2064	61
	2.74	0.10	0.09	2.75	0.06	2074	51
	2.89	0.20	0.19	2.75	0.06	2085	40
Trough	2.88[a,b]	0.55	0.46	2.73	0.05	966	1159
CTD 909	2.82[a,b]	0.11	0.11	2.74	0.05	1163	962
	2.86[a,b]	0.38	0.33	2.74	0.05	1358	767
	2.80[b]	0.17	0.16	2.75	0.05	1752	373
	2.80[b]	0.14	0.13	2.75	0.05	1946	179
	2.76[b]	0.11	0.11	2.75	0.06	2067	58
	2.73[b]	0.09	0.09	2.75	0.06	2077	48
	2.91[b]	0.15	0.15	2.75	0.06	2087	38
	2.65[b]	0.08	0.07	2.75	0.06	2097	28
	2.61[b]	0.05	0.05	2.75	0.06	2107	18
Slope	3.10[b]	0.38	0.34	2.73	0.05	754	797
CTD 920	2.82[b]	0.38	0.33	2.73	0.05	952	599
	2.82[b]	0.10	0.10	2.74	0.05	1152	399
	2.83[b]	0.23	0.21	2.74	0.05	1352	199
	3.12[b]	0.87	0.68	2.74	0.05	1452	99
	3.00[b]	0.24	0.22	2.74	0.05	1503	48
	2.98[b]	0.30	0.28	2.74	0.05	1513	38
	2.89[b]	0.15	0.14	2.74	0.05	1523	28
	2.72[b]	0.15	0.14	2.74	0.05	1533	18
	2.94[b]	0.53	0.45	2.74	0.05	1544	7
Slope	2.91	0.11	0.11	2.73	0.05	842	924
CTD 923	2.72	0.36	0.32	2.74	0.05	970	796
	3.01	0.25	0.23	2.74	0.05	1042	724
	2.75	0.10	0.09	2.74	0.05	1441	325
	2.89	0.20	0.18	2.75	0.05	1641	125
	3.03	0.21	0.20	2.75	0.05	1691	75
	3.04[b]	0.23	0.21	2.75	0.05	1701	65
	2.92[b]	0.29	0.26	2.75	0.05	1711	55
	2.99[b]	0.55	0.47	2.75	0.05	1721	45

Table A1 (*continued*)

Station ID	Total ^{234}Th (dpm L^{-1})	+1SD (dpm L^{-1})	−1SD (dpm L^{-1})	^{238}U (dpm L^{-1})	1SD (dpm L^{-1})	Depth (m)	Height above seafloor (m)
	2.94[b]	0.51	0.44	2.75	0.05	1731	35
Trough	2.85	0.27	0.24	2.74	0.05	958	1167
CTD 935	2.93	0.08	0.08	2.74	0.05	1162	963
	3.02	0.66	0.54	2.74	0.05	1336	789
	2.75	0.25	0.23	2.75	0.05	1736	389
	2.76	0.10	0.10	2.75	0.06	2006	119
	2.89	0.24	0.22	2.75	0.06	2056	69
	2.77[a]	0.48	0.41	2.75	0.06	2066	59
	2.92[a]	0.18	0.17	2.75	0.06	2076	49
	2.87[a]	0.24	0.23	2.75	0.06	2086	39
	2.91	0.48	0.42	2.75	0.06	2096	29
Trough	2.82	0.37	0.33	2.74	0.05	950	1175
CTD 937	2.91	0.28	0.25	2.74	0.05	1150	975
	2.83	0.37	0.33	2.74	0.05	1349	776
	2.83	0.08	0.08	2.75	0.05	1750	375
	2.82	0.19	0.18	2.75	0.06	2005	120
	2.57	0.41	0.35	2.75	0.06	2056	69
	2.88	0.09	0.09	2.75	0.06	2066	59
	2.67	0.11	0.11	2.75	0.06	2077	48
	2.78	0.15	0.14	2.75	0.06	2087	38
	2.73	0.07	0.07	2.75	0.06	2096	29
Slope	2.68	0.62	0.51	2.74	0.05	854	917
CTD 946	2.63	0.16	0.15	2.74	0.05	1052	719
	3.06	0.35	0.32	2.74	0.05	1251	520
	2.74	0.07	0.06	2.74	0.05	1450	321
	2.53	0.19	0.17	2.75	0.05	1651	120
	3.17	0.49	0.43	2.75	0.05	1700	71
	3.00	0.46	0.40	2.75	0.05	1711	60
	2.50	0.29	0.26	2.75	0.05	1721	50
	2.85	0.19	0.18	2.75	0.05	1731	40
	2.83	0.28	0.26	2.75	0.05	1740	31
Slope	2.95	0.20	0.18	2.74	0.05	854	917
CTD 950	2.81	0.19	0.18	2.74	0.05	1054	717
	2.83	0.33	0.30	2.74	0.05	1253	518
	2.90	0.08	0.08	2.74	0.05	1452	319
	2.85	0.54	0.46	2.75	0.05	1652	119
	3.02	0.72	0.58	2.75	0.05	1702	69
	2.73	0.14	0.13	2.75	0.05	1712	59
	2.91	0.07	0.07	2.75	0.05	1722	49
	2.76	0.08	0.07	2.75	0.05	1732	39
	2.84	0.14	0.13	2.75	0.05	1742	29

For details on the calculation of ^{234}Th and ^{238}U uncertainties see Section 2.3.2 of main text. SD: standard deviation; dpm: disintegrations per minute.
[a] Data corrected for short-lived contamination, possibly caused by ^{224}Ra and ^{223}Ra.
[b] Samples belonging to the batch of filters (F2) with higher backgrounds.

Table A2
Compilation of sampling depths and heights above the seafloor, and of particulate organic carbon (POC) and nitrogen (PON) amounts per filter, plus filtered volumes of the experiment investigating the effect of adsorption of dissolved organic matter onto the GF/F filters.

Station ID	POC (mg filter^{-1})	PON (mg filter^{-1})	Filtered volume (L)	Depth (m)	Height above seafloor (m)
Rhodes Basin	0.0625	0.0021	0.1	2001	2428
CTD 881	0.0397	0.0021	0.1	2001	2428
	0.0620	0.0021	0.2	2001	2428
	0.0433	0.0021	0.2	2001	2428
	0.1031	0.0027	0.5	2001	2428
	0.0525	0.0021	0.5	2001	2428
	0.0755	0.0021	1.0	2001	2428
	0.0687	0.0030	1.0	2001	2428
	0.0905	0.0036	2.0	2001	2428
	0.0634	0.0036	2.0	2001	2428
	0.1304	0.0059	5.0	2001	2428

Table A2 (*continued*)

Station ID	POC (mg filter^{-1})	PON (mg filter^{-1})	Filtered volume (L)	Depth (m)	Height above seafloor (m)
	0.1474	0.0060	5.0	2001	2428
	0.2357	0.0086	10.0	2001	2428

For details of the experiment see section 2.3.3.

Table A3
Compilation of sampling depths and heights above the seafloor, and of adsorption-corrected particulate organic carbon (POC) and nitrogen (PON) concentrations, plus filtered volumes of all seamount samples.

Station ID	POC ($\mu g\,L^{-1}$)	PON ($\mu g\,L^{-1}$)	Filtered volume (L)	Depth (m)	Height above seafloor (m)
Slope	13.55	1.06	8.0	964	807
CTD 892	4.79	0.63	8.0	1159	612
	9.86	0.79	8.0	1355	416
	2.99	0.31	8.0	1551	220
	11.94	0.94	8.0	1650	121
	8.45	0.24	8.0	1702	69
	5.81	0.61	8.0	1711	60
	18.71	1.17	8.0	1722	49
	6.77	0.51	8.0	1731	40
	2.36	0.38	8.0	1742	25
Slope	14.76	1.65	8.0	967	804
CTD 893	4.47	0.52	8.0	1160	611
	12.09	0.60	8.0	1359	412
	9.82	1.29	8.0	1554	217
	7.98	0.73	8.0	1651	120
	11.70	1.00	8.0	1702	69
	11.85	0.76	8.0	1711	60
	9.66	1.15	8.0	1720	51
	6.21	0.82	8.0	1731	40
	5.66	0.79	8.0	1742	29
Trough	13.65	1.54	8.0	965	1160
CTD 907	4.03	0.37	8.0	1161	964
	3.40	0.34	8.0	1357	768
	4.82	0.46	8.0	1752	373
	6.53	0.51	8.0	1948	177
	5.48	0.32	8.0	2044	81
	8.05	0.30	8.0	2054	71
	5.75	0.32	8.0	2064	61
	2.54	0.33	8.0	2074	51
	4.55	0.52	8.0	2085	40
Trough	7.10	0.71	8.0	966	1159
CTD 909	6.29	0.56	8.0	1163	962
	7.55	0.34	8.0	1358	767
	11.38	0.71	8.0	1752	373
	19.24	2.81	8.0	1946	179
	9.08	0.75	8.0	2067	58
	3.86	0.35	8.0	2077	48
	11.00	1.10	8.0	2087	38
	2.26	0.45	8.0	2097	28
	4.12	0.55	8.0	2107	18
Slope	19.67	1.17	8.0	754	797
CTD 920	2.21	0.31	8.0	952	599
	n.d.	n.d.	8.0	1152	399
	4.59	0.69	8.0	1352	199
	7.38	0.72	8.0	1452	99
	3.81	0.54	8.0	1503	48
	5.69	0.48	8.0	1513	38
	22.69	1.03	8.0	1523	28
	9.62	0.86	8.0	1533	18
	n.d.	n.d.	8.0	1544	7
Slope	11.80	0.61	7.6	842	924
CTD 923	8.64	0.67	8.0	970	796
	n.d.	n.d.	8.0	1042	724
	7.23	0.87	8.0	1441	325

Table A3 (*continued*)

Station ID	POC ($\mu g\,L^{-1}$)	PON ($\mu g\,L^{-1}$)	Filtered volume (L)	Depth (m)	Height above seafloor (m)
	7.92	0.32	8.0	1641	125
	7.12	0.59	8.0	1691	75
	20.20	0.78	8.0	1701	65
	7.96	0.58	7.6	1711	55
	7.30	0.54	8.0	1721	45
	11.53	0.28	8.0	1731	35
Trough	22.69	1.84	8.0	958	1167
CTD 935	5.95	0.57	8.0	1162	963
	3.50	0.40	8.0	1336	789
	0.00	0.00	0.4	1736	389
	5.75	0.64	8.0	2006	119
	4.63	0.44	8.0	2056	69
	16.89	0.45	8.0	2066	59
	7.42	0.82	8.0	2076	49
	6.86	0.83	8.0	2086	39
	8.64	0.67	8.0	2096	29
Trough	12.42	1.80	8.0	950	1175
CTD 937	16.26	1.57	8.0	1150	975
	9.66	0.66	8.0	1349	776
	5.40	0.63	8.0	1750	375
	7.26	0.70	8.0	2005	120
	6.43	0.67	8.0	2056	69
	5.16	0.70	8.0	2066	59
	11.80	0.93	8.0	2077	48
	6.10	0.72	8.0	2087	38
	15.05	1.01	8.0	2096	29
Slope	6.33	0.47	8.0	854	917
CTD 946	4.82	0.35	8.0	1052	719
	2.91	0.20	8.0	1251	520
	13.31	0.61	8.0	1450	321
	9.67	0.55	8.0	1651	120
	23.22	1.53	8.0	1700	71
	7.55	0.67	8.0	1711	60
	14.84	0.87	8.0	1721	50
	17.75	1.26	8.0	1731	40
	17.40	0.86	8.0	1740	31
Slope	0.92	0.31	8.0	854	917
CTD 950	2.16	0.33	7.7	1054	717
	2.32	0.28	8.0	1253	518
	4.97	0.36	8.0	1452	319
	16.67	0.35	8.0	1652	119
	11.62	0.38	8.0	1702	69
	8.14	0.51	8.0	1712	59
	11.14	0.37	8.0	1722	49
	17.37	0.50	8.0	1732	39
	16.56	0.82	8.0	1742	29

n.d.: not determined.

References

Aloisi, G., Wallmann, K., Haese, R.R., Saliège, J.-F., 2004. Chemical, biological and hydrological controls on the ^{14}C content of cold seep carbonate crusts: numerical modeling and implications for convection at cold seeps. Chemical Geology 213, 359–383.

Bacon, M.P., Anderson, R.F., 1982. Distribution of thorium isotopes between dissolved and particulate forms in the deep sea. Journal of Geophysical Research 87, 2045–2056.

Bacon, M.P., Rutgers van der Loeff, M.M., 1989. Removal of ^{234}Th by scavenging in the bottom nepheloid layer of the ocean. Earth and Planetary Science Letters 92, 157–164.

Balmforth, N.J., Ierley, G.R., Young, W.R., 2002. Tidal conversion by subcritical topography. Journal of Physical Oceanography 32, 2900–2914.

Beckmann, A., Mohn, C., 2002. The upper ocean circulation at Great Meteor Seamount. Part II: retention potential of the seamount-induced circulation. Ocean Dynamics 52, 194–204.

Broecker, W.S., 2008. Excess sediment ^{230}Th: transport along the sea floor or enhanced water column scavenging? Global Biogeochemical Cycles 22 (1), GB1006.

Cacchione, D.A., Pratson, L.F., Ogston, A.S., 2002. The shaping of continental slopes by internal tides. Science 296, 724–727.

Castro, C.G., Pérez, F.F., Holley, S.E., Ríos, A.F., 1998. Chemical characterization and modelling of water masses in the Northeast Atlantic. Progress in Oceanography 41, 249–279.

Chapman, D.C., Haidvogel, D.B., 1992. Formation of Taylor caps over a tall isolated seamount in a stratified ocean. Geophysical and Astrophysical Fluid Dynamics 64, 31–65.

Chen, J.H., Edwards, R.L., Wasserburg, G.J., 1986. ^{238}U, ^{234}U and ^{232}Th in seawater. Earth and Planetary Science Letters 80 (3–4), 241–251.

DeMaster, D.J., Brewster, D.C., McKee, B.A., Nittrouer, C.A., 1991. Rates of particle scavenging, sediment reworking and longitudinal ripple formation at the HEBBLE site based on measurements of ^{234}Th and ^{210}Pb. Marine Geology 99, 423–444.

Dickson, R.R., Gould, W.J., Müller, T.J., Maillard, C., 1985. Estimates of the mean circulation in the deep (>2,000 m) layer of the Eastern North Atlantic. Progress in Oceanography 14, 103–127.

Dickson, R.R., McCave, I.N., 1986. Nepheloid layers on the continental slope west of Porcupine Bank. Deep-Sea Research 33 (6), 791–818.

Egbert, G.D., Ray, R.D., Bills, B.G., 2004. Numerical modeling of the global semidiurnal tide in the present day and in the last glacial maximum. Journal of Geophysical Research 109, C03003.

Egbert, G.D., Erofeeva, S., 2002. Efficient inverse modeling of barotropic ocean tides. Journal of Atmospheric and Oceanic Technology 19, 183–204.

Firing, E., Ranada, J., Caldwell, S., 1995. Processing ADCP data with the CODAS Software System, Version 3.1, University of Hawaii, Honolulu, HI.

Francois, R., Frank, M., Rutgers van der Loeff, M.M., Bacon, M.P., 2004. ^{230}Th normalization: an essential tool for interpreting sedimentary fluxes during the late Quaternary. Paleoceanography 19, PA1018.

Francois, R., Frank, M., Rutgers van der Loeff, M.M., Bacon, M.P., Geibert, W., Kienast, S., Anderson, R.F., Bradtmiller, L., Chase, Z., Henderson, G., Marcantonio, F., Allen, S.E., 2004. Comment on "Do geochemical estimates of sediment focusing pass the sediment test in the equatorial Pacific?" by M. Lyle et al. Paleoceanography 22, PA1216.

Gardner, W.D., Richardson, M.J., Carlson, C.A., Hansell, D., Mishonov, A.V., 2003. Determining true particulate organic carbon: bottles, pumps and methodologies. Deep-Sea Research II 50, 655–674.

Garrett, C., Kunze, E., 2007. Internal tide generation in the deep ocean. Annual Review of Fluid Mechanics 39, 57–87.

Geibert, W., Usbeck, R., 2004. Adsorption of thorium and protactinium onto different particle types: experimental findings. Geochimica et Cosmochimica Acta 68 (7), 1489–1501.

Goldner, D.R., Chapman, D.C., 1997. Flow and particle motion induced above a tall seamount by steady and tidal background currents. Deep-Sea Research I 44 (5), 719–744.

Gould, W.J., Hendry, R., Huppert, H.E., 1981. An abyssal topographic experiment. Deep-Sea Research 28A (5), 409–440.

Gross, T.F., Williams, A.J., 1991. Characterization of deep-sea storms. Marine Geology 99 (3–4), 281–301.

Haese, R.R., Hensen, C., de Lange, G.J., 2006. Pore water geochemistry of Eastern Mediterranean mud volcanoes: implications for fluid transport and fluid origin. Marine Geology 225, 191–208.

Honeyman, B.D., Balistrieri, L.S., Murray, J.W., 1988. Oceanic trace-metal scavenging—the importance of particle concentration. Deep-Sea Research 35A (2), 227–246.

Inthorn, M., Rutgers van der Loeff, M., Zabel, M., 2006. A study of particle exchange at the sediment–water interface in the Benguela upwelling area based on ^{234}Th/^{238}U disequilibrium. Deep-Sea Research I 53, 1742–1761.

Khatiwala, S., 2003. Generation of internal tides in an ocean of finite depth: analytical and numerical calculations. Deep-Sea Research I 50, 3–21.

Kienast, S.S., Kienast, M., Mix, A.C., Calvert, S.E., François, R., 2007. ^{230}Th normalized particle flux and sediment focusing in the Panama Basin region during the last 30,000 years. Paleoceanography 22, PA2213.

Klein, H., Mittelstaedt, E., 1992. Currents and dispersion in the abyssal Northeast Atlantic. Results from the NOAMP field program. Deep-Sea Research 39 (10), 1727–1745.

Lampitt, R.S., 1985. Evidence for the seasonal deposition of detritus to the deep-sea floor and its subsequent resuspension. Deep-Sea Research 32A (8), 885–897.

Lampitt, R.S., Bett, B.J., Kiriakoulakis, K., Popova, E.E., Ragueneau, O., Vangriesheim, A., Wolff, G.A., 2001. Material supply to the abyssal seafloor in the Northeast Atlantic. Progress in Oceanography 50, 27–63.

Legg, S., Huijts, K.M.H., 2006. Preliminary simulations of internal waves and mixing generated by finite amplitude tidal flow over isolated topography. Deep-Sea Research II 53 (1–2), 140–156.

Liu, Z., Stewart, G., Cochran, J.K., Lee, C., Armstrong, R.A., Hirschberg, D.J., Gasser, B., Miquel, J.-C., 2005. Why do POC concentrations measured using Niskin bottle collections sometimes differ from those using in-situ pumps? Deep-Sea Research I 52, 1324–1344.

Llewellyn Smith, S.G., Young, W.R., 2002. Conversion of the barotropic tide. Journal of Physical Oceanography 32, 1554–1566.

Loncke, L., Gaullier, V., Mascle, J., Vendeville, B., Camera, L., 2006. The Nile deep-sea fan: an example of interacting sedimentation, salt tectonics, and inherited subsalt paleotopographic features. Marine and Petroleum Geology 23, 297–315.

Lyle, M., Mitchell, N., Pisias, N., Mix, A., Martinez, J.I., Paytan, A., 2005. Do geochemical estimates of sediment focusing pass the sediment test in the equatorial Pacific? Paleoceanography 20, PA1005.

Lyle, M., Pisias, N., Paytan, A., Martinez, J.I., Mix, A., 2007. Reply to comment by R. Francois et al. on "Do geochemical estimates of sediment focusing pass the sediment test in the equatorial Pacific?": further explorations of ^{230}Th normalization. Paleoceanography 22, PA1217.

Lynch-Stieglitz, J., Adkins, J.F., Curry, W.B., Dokken, T., Hall, I.R., Herguera, J.C., Hirschi, J.J.-M., Ivanova, E.V., Kissel, C., Marchal, O., Marchitto, T.M., McCave, I.N., McManus, J.F., Mulitza, S., Ninnemann, U., Peeters, F., Yu, E.-F., Zahn, R., 2007. Atlantic meridional overturning circulation during the Last Glacial Maximum. Science 316, 66–69.

McCartney, M.S., 1992. Recirculating components to the deep boundary current of the northern North Atlantic. Progress in Oceanography 29, 283–383.

McCave, I.N., Hall, I.R., 2006. Size sorting in marine muds: processes, pitfalls, and prospects for paleoflow-speed proxies. Geochemistry, Geophysics, Geosystems 7 (10), Q10N05.

Menzel, D.W., 1966. Bubbling of sea water and the production of organic particles: a re-evaluation. Deep-Sea Research 13, 963–966.

Mittelstaedt, E., Bock, M., Bork, I., Klein, H., Nies, H., Schauer, U., 1986. Nordost-Atlantisches Monitoring Programm: Ausbreitungsbedingungen für Stoffe in grossen Ozeantiefen. Deutsches Hydrographisches Institut, Hamburg, p. 202.

Mohn, C., Beckmann, A., 2002. The upper ocean circulation at Great Meteor Seamount. Part I: structure of density and flow fields. Ocean Dynamics 52, 179–193.

Montenegro, Á., Eby, M., Weaver, A.J., Jayne, S.R., 2007. Response of a climate model to tidal mixing parameterization under present day and last glacial maximum conditions. Ocean Modelling 19, 125–137.

Moran, S.B., Charette, M.A., Pike, S.M., Wicklund, C.A., 1999. Differences in seawater particulate organic carbon concentration in samples collected using small- and large-volume methods: the importance of DOC adsorption to the filter blank. Marine Chemistry 67, 33–42.

Nilsson, J., Broström, G., Walin, G., 2003. The thermohaline circulation and vertical mixing: does weaker density stratification give stronger overturning? Journal of Physical Oceanography 33, 2781–2795.

Nycander, J., 2005. Generation of internal waves in the deep ocean by tides. Journal of Geophysical Research 110, C10028.

Olu-Le Roy, K., Sibuet, M., Fiala-Médioni, A., Gofas, S., Salas, C., Mariotti, A., Foucher, J.-P., Woodside, J., 2004. Cold seep communities in the deep Eastern Mediterranean Sea: composition, symbiosis and spatial distribution on mud volcanoes. Deep-Sea Research I 51, 1915–1936.

Pates, J.M., Muir, G.K.P., 2007. U–salinity relationships in the Mediterranean: implications for ^{234}Th:^{238}U particle flux studies. Marine Chemistry 106 (3–4), 530–545.

Quigley, M.S., Santschi, P.H., Guo, L., Honeyman, B.D., 2001. Sorption irreversibility and coagulation behaviour of ^{234}Th with marine organic matter. Marine Chemistry 76, 27–45.

Ray, R.D., 2001. Internal tides. In: Steele, J.H., Thorpe, S.A., Turekian, K.K. (Eds.), Encyclopedia of Ocean Sciences, vol. 3, I-M. Academic Press, San Diego, pp. 1327–1335.

Robinson, A.R., Golnaraghi, M., Leslie, W.G., Artegiani, A., Hecht, A., Lazzoni, E., Michelato, A., Sansone, E., Theocharis, A., Unluata, U., 1991. The Eastern Mediterranean general-circulation-features, structure and variability. Dynamics of Atmospheres and Oceans 15 (3–5), 215–240.

Rutgers van der Loeff, M.M., Moore, W.S., 1999. Determination of natural radioactive tracers. In: Grasshoff, K., Kremling, K., Ehrhardt, M. (Eds.), Methods of Seawater Analysis. Wiley-VCH, Weinheim, pp. 365–397.

Rutgers van der Loeff, M.M., Meyer, R., Rudels, B., Rachor, E., 2002. Resuspension and particle transport in the benthic nepheloid layer in and near Fram Strait in relation to faunal abundances and ^{234}Th depletion. Deep-Sea Research I 49, 1941–1958.

Rutgers van der Loeff, M., Sarin, M.M., Baskaran, M., Benitez-Nelson, C., Buesseler, K.O., Charette, M., Dai, M., Gustafsson, Ö., Masque, P., Morris, P.J., Orlandini, K., Rodriguez y Baena, A., Savoye, N., Schmidt, S., Turnewitsch, R., Vöge, I., Waples, J.T., 2006. A review of present techniques and methodological advances in analyzing ^{234}Th in aquatic systems. Marine Chemistry 100, 190–212.

Seibold, E., Berger, W.H., 1993. The Seafloor—An Introduction to Marine Geology, third ed. Springer, Berlin, Heidelberg, New York, p. 356.

Smith, W.H.F., Sandwell, D.T., 1997. Global sea floor topography from satellite altimetry and ship depth soundings. Science 277, 1956–1962.

St. Laurent, L.C., Garrett, C., 2002. The role of internal tides in mixing the deep ocean. Journal of Physical Oceanography 32, 2882–2899.

ten Veen, J.H., Woodside, J.M., Zitter, T.A.C., Dumont, J.F., Mascle, J., Volkonskaia, A., 2004. Neotectonic evolution of the Anaximander

Mountains at the junction of the Hellenic and Cyprus arcs. Tectonophysics 391, 35–65.
Turnewitsch, R., Reyss, J.L., Nycander, J., Waniek, J.J., Lampitt, R.S., 2008. Internal tides and sediment dynamics in the deep sea—evidence from radioactive Th-234/U-238 disequilibria. Deep-Sea Research Part I 55, 1727–1747.
Turnewitsch, R., Reyss, J.L., Chapman, D.C., Thomson, J., Lampitt, R.S., 2004. Evidence for a sedimentary fingerprint of an asymmetric flow field surrounding a short seamount. Earth and Planetary Science Letters 222 (3–4), 1023–1036.
Turnewitsch, R., Springer, B., 2001. Do bottom mixed layer influence ^{234}Th dynamics in the abyssal near-bottom water column? Deep-Sea Research I 48, 1279–1307.
Turnewitsch, R., Springer, B.M., Kiriakoulakis, K., Vilas, J.C., Aristegui, J., Wolff, G., Peine, F., Werk, S., Graf, G., Waniek, J.J., 2007. Determination of particulate organic carbon (POC) in seawater: the relative methodological importance of artificial gains and losses in two glass-fiber-filter-based techniques. Marine Chemistry 105 (3–4), 208–228.
van Aken, H.M., 2007. The Oceanic Thermohaline Circulation—An Introduction. Springer, New York, p. 326.
Vangriesheim, A., Springer, B., Crassous, P., 2001. Temporal variability of near-bottom particle resuspension and dynamics at the Porcupine Abyssal Plain, Northeast Atlantic. Progress in Oceanography 50, 123–145.
van Haren, H., 2007. Inertial and tidal shear variability above Reykjanes Ridge. Deep-Sea Research I 54, 856–870.
Verardo, D.J., Froelich, P.N., Mcintyre, A., 1990. Determination of organic-carbon and nitrogen in marine-sediments using the Carlo-Erba-Na-1500 analyzer. Deep-Sea Research Part A 37 (1), 157–165.
Vlasenko, V., Stashchuk, N., Hutter, K., 2005. Baroclinic Tides—Theoretical Modeling and Observational Evidence. Cambridge University Press, Cambridge, p. 351.
Walsh, I., Fisher, K., Murray, D., Dymond, J., 1988. Evidence for resuspension of rebound particles from near-bottom sediment traps. Deep-Sea Research 35 (1), 59–70.
Walsh, I.D., 1992. Large aggregate flux and fate at the seafloor: diagensis during the rebound process. In: Rowe, G.T., Pariente, V. (Eds.), Deep-Sea Food Chains and the Global Carbon Cycle. Kluwer Academic Publishers, Dordrecht, pp. 365–373.
Waples, J.T., Orlandini, K.A., Weckerly, K.M., Edgington, D.N., Klump, J.V., 2003. Measuring low concentrations of ^{234}Th in water and sediment. Marine Chemistry 80, 265–281.
Wunsch, C., Ferrari, R., 2004. Vertical mixing, energy, and the general circulation of the oceans. Annual Review of Fluid Mechanics 36, 281–314.
Ziervogel, K., Bohling, B., 2003. Sedimentological parameters and erosion behaviour of submarine coastal sediments in the south-western Baltic Sea. Geomarine Letters 23 (1), 43–52.
Zitter, T.A.C., Huguen, C., Woodside, J.M., 2005. Geology of mud volcanoes in the Eastern Mediterranean from combined sidescan sonar and submersible surveys. Deep-Sea Research I 52, 457–475.